Defense Nuclear Agency
Alexandria, VA 22310-3398

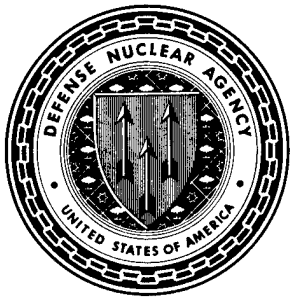

DNA-TR-95-95

Crater Volume–Relative Contributions of Flow, Compaction and Elastic Transport

John G. Trulio
Applied Theory, Inc.
930 South La Brea Avenue
Suite 2
Los Angeles, CA 90036

December 1997

Technical Report

CONTRACT No. DNA 001-88-C-0130

DISCLAIMER

The views and conclusions contained in this document are those of the authors and should not be interpreted as necessarily representing the official policies, either expressed or implied of the Defense Special Weapons Agency or the U. S. Government.

DESTRUCTION NOTICE:

Destroy this report when it is no longer needed.
Do not return to sender.

PLEASE NOTIFY THE DEFENSE SPECIAL WEAPONS AGENCY, ATTN: CSTI, 6801TELEGRAPH ROAD, ALEXANDRIA, VA 22310-3398, IF YOUR ADDRESS IS INCORRECT, IF YOU WISH IT DELETED FROM THE DISTRIBUTION LIST, OR IF THE ADDRESSEE IS NO LONGER EMPLOYED BY YOUR ORGANIZATION.

DISTRIBUTION LIST UPDATE

This mailer is provided to enable DSWA to maintain current distribution lists for reports. (We would appreciate your providing the requested information.)

☐ Add the individual listed to your distribution list.

☐ Delete the cited organization/individual.

☐ Change of address.

NOTE:
Please return the mailing label from the document so that any additions, changes, corrections or deletions can be made easily. For distribution cancellation or more information call DSWA/IMAS (703) 325-1036.

NAME: _____

ORGANIZATION: _____

OLD ADDRESS	CURRENT ADDRESS
_____	_____
_____	_____
_____	_____

TELEPHONE NUMBER: ( ) _____

DSWA PUBLICATION NUMBER/TITLE	CHANGES/DELETIONS/ADDITIONS, etc.) *(Attach Sheet if more Space is Required)*
_____	_____
_____	_____
_____	_____

DSWA OR OTHER GOVERNMENT CONTRACT NUMBER: _____

CERTIFICATION OF NEED-TO-KNOW BY GOVERNMENT SPONSOR (if other than DSWA):

SPONSORING ORGANIZATION: _____

CONTRACTING OFFICER OR REPRESENTATIVE: _____

SIGNATURE: _____

CUT HERE AND RETURN

DEFENSE SPECIAL WEAPONS AGENCY
ATTN: IMAS
6801 TELEGRAPH ROAD
ALEXANDRIA, VA 22310-3398

DEFENSE SPECIAL WEAPONS AGENCY
ATTN: IMAS
6801 TELEGRAPH ROAD
ALEXANDRIA, VA 22310-3398

REPORT DOCUMENTATION PAGE

Form Approved
OMB No. 0704-0188

1. AGENCY USE ONLY (Leave blank)	2. REPORT DATE	3. REPORT TYPE AND DATES COVERED
	971201	Technical 880630 - 950918

4. TITLE AND SUBTITLE
Crater Volume–Relative Contributions of Flow, Compaction and Elastic Transport

5. FUNDING NUMBERS
C - DNA 001-88-C-0130
PE - 62715H
PR - RS
TA - RB
WU - DH051270

6. AUTHOR(S)
John G. Trulio

7. PERFORMING ORGANIZATION NAME(S) AND ADDRESS(ES)
Applied Theory, Inc.
930 South La Brea Avenue
Suite 2
Los Angeles, CA 90036

8. PERFORMING ORGANIZATION REPORT NUMBER
ATR-95-72-1

9. SPONSORING/MONITORING AGENCY NAME(S) AND ADDRESS(ES)
Defense Special Weapons Agency
6801 Telegraph Road
Alexandria, VA 22310-3398
WEP/Ullrich

10. SPONSORING/MONITORING AGENCY REPORT NUMBER
DNA-TR-95-95

11. SUPPLEMENTARY NOTES
This work was sponsored by the Defense Special Weapons Agency under RDT&E RMC Code B4662D RS RB 00072 SPWE 4400A 25904D.

12a. DISTRIBUTION/AVAILABILITY STATEMENT
Approved for public release; distribution is unlimited.

12b. DISTRIBUTION CODE

13. ABSTRACT *(Maximum 200 words)*

As now modeled, near-surface (and contained) bursts make room for craters (cavities) mainly by missile-ejection, flow of otherwise-elastic material, and compaction. An exact solution discovered here for locking solids admits elasticity, plasticity and compaction: For spherical bursts, a cavity-radius-dependent pressure P_c on the wall then forces nearby material to flow (and compact) until, at radii $>r_{ep}$, falling shock stress precludes shear failure. Flow ends; material freezes compressive hoop stress out to r_{ep}, beyond r_{ep}, a compressive elastic wave moves ever outward. Exactly that field develops in a half space whose hemispherical crater bears pressure P_c, while the (flat) balance of its surface bears the spherical field's hoop stress. Such ground loading is no surface-burst replica, but is compressive and decays as it spreads – and so drives a surface-burst-related cratering field.

After freezing occurs, stiffness is more apt than rigidity within radius r_{ep}. An elastic wave due to overpressure's fall to zero at the ground surface, thus adds in to produce our terminal field. Out to r_{ep}, part of the compacted-out volume then reverts to elastic compression; the crater's volume becomes a sum of volumes due to compaction and elastic compression out to r_{ep}, plus volume trapped in the elastic wave moving outward from r_{ep}. For six media whose elastic moduli reflect tests of Pacific coral, the fraction of crater volume in that wave ran from 1/6 to 1/3.

14. SUBJECT TERMS
Craters
Elastic Transport
Flow
Compaction

15. NUMBER OF PAGES
56

16. PRICE CODE

17. SECURITY CLASSIFICATION OF REPORT	18. SECURITY CLASSIFICATION OF THIS PAGE	19. SECURITY CLASSIFICATION OF ABSTRACT	20. LIMITATION OF ABSTRACT
UNCLASSIFIED	UNCLASSIFIED	UNCLASSIFIED	SAR

NSN 7540-280-5500

Standar d Form 298 ((rev. 2-89)
Precribed by ANSI Sta. 239-18
298-102

CLASSIFIED BY:

N/A since Unclassified.

DECLASSIFY ON:

N/A since Unclassified.

CONVERSION TABLE

Conversion factors for U.S. Customary to metric (SI) units of measurement.

MULTIPLY → / ← TO GET	BY → / ← BY	TO GET → / ← DIVIDE
angstrom	1.000 000 X E -10	meters (m)
atmosphere (normal)	1.013 25 X E +2	kilo pascal (kPa)
bar	1.000 000 X E +2	kilo pascal (kPa)
barn	1.000 000 X E -28	meter^2 (m^2)
British thermal unit (thermochemical)	1.054 350 X E +3	joule (J)
calorie (thermochemical)	4.184 000	joule (J)
cal (thermochemical/cm^2)	4.184 000 X E -2	mega joule/m^2 (MJ/m^2)
curie	3.700 000 X E +1	*giga becquerel (GBq)
degree (angle)	1.745 329 X E -2	radian (rad)
degree Fahrenheit	$t_k = (t^\circ f + 459.67)/1.8$	degree kelvin (K)
electron volt	1.602 19 X E -19	joule (J)
erg	1.000 000 X E -7	joule (J)
erg/second	1.000 000 X E -7	watt (W)
foot	3.048 000 X E -1	meter (m)
foot-pound-force	1.355 818	joule (J)
gallon (U.S. liquid)	3.785 412 X E -3	meter^3 (m^3)
inch	2.540 000 X E -2	meter (m)
jerk	1.000 000 X E +9	joule (J)
joule/kilogram (J/kg) radiation dose absorbed	1.000 000	Gray (Gy)
kilotons	4.183	terajoules
kip (1000 lbf)	4.448 222 X E +3	newton (N)
kip/inch^2 (ksi)	6.894 757 X E +3	kilo pascal (kPa)
ktap	1.000 000 X E +2	newton-second/m^2 ($N-s/m^2$)
micron	1.000 000 X E -6	meter (m)
mil	2.540 000 X E -5	meter (m)
mile (international)	1.609 344 X E +3	meter (m)
ounce	2.834 952 X E -2	kilogram (kg)
pound-force (lbs avoirdupois)	4.448 222	newton (N)
pound-force inch	1.129 848 X E -1	newton-meter (N·m)
pound-force/inch	1.751 268 X E +2	newton/meter (N/m)
pound-force/foot^2	4.788 026 X E -2	kilo pascal (kPa)
pound-force/inch^2 (psi)	6.894 757	kilo pascal (kPa)
pound-mass (lbm avoirdupois)	4.535 924 X E -1	kilogram (kg)
pound-mass-foot^2 (moment of inertia)	4.214 011 X E -2	kilogram-meter^2 ($kg·m^2$)
pound-mass/foot^3	1.601 846 X E +1	kilogram/meter^3 (kg/m^3)
rad (radiation dose absorbed)	1.000 000 X E -2	**Gray (Gy)
roentgen	2.579 760 X E -4	coulomb/kilogram (C/kg)
shake	1.000 000 X E -8	second (s)
slug	1.459 390 X E +1	kilogram (kg)
torr (mm Hg, 0° C)	1.333 22 X E -1	kilo pascal (kPa)

*The becquerel (Bq) is the SI unit of radioactivity; 1 Bq = 1 event/s.
**The Gray (GY) is the SI unit of absorbed radiation.

TABLE OF CONTENTS

FIGURES

SECTION 1
BACKGROUND AND OUTLINE

"The bombs bursting in air" seldom produce craters, but most other explosions do. Hence, anent weapons effects – always of vital concern to the DoD – few subjects have received as much attention as craters and cratering (witness CARES). Two decades ago, the DoD had already sponsored at least 25 nuclear explosive events and 150 of conventional type, wholly or in part to study craters (Cooper, 1976; a partial list), plus a larger number of "first principles" computer simulations of such events. Indeed, as recent interest in tunnel damage illustrates, cratering remains basic among weapon-effects even for conventional weapons.

Cratering studies (especially theoretical ones) have identified several processes whereby craters form ("cratering mechanisms"). These range from void closure ("compaction"), the creation of free-flying rock/soil missiles (ejecta "throwout" and "fallback"), and permanent displacement during shear failure ("flow") – which occur widely – to more subtle and specialized processes (e.g., "piping;" at wet, atoll-like sites, rock particles in slurries are forced upward through fissures by geostatic or other loads, whereupon currents in otherwise clear water carry them away). Highly specialized mechanisms abound, because most of the myriad refinements to models of the mechanical properties of a site have some effect on permanent burst-induced volume changes in site materials.

Special and subtle mechanisms tend to be more speculative and less effective than those of obvious widespread occurrence (such as compaction). New *obvious* mechanisms therefore hold relatively great potential for explaining crater formation, and for entering decisively into cratering theories. Yet, at this late date, "new" and "obvious" are almost contradictory terms. Both apply nonetheless to a nearly universal mechanism ("obvious," after the fact) that surfaced just a few years ago: transport of crater volume to very great distances by elastic waves of low (even seismic) amplitude. Accordingly, crater-volume budgets need to specify, at the least (i.e., ignoring special subtle mechanisms), the contributions to total volume from throwout, compaction, flow, *and* elastic volume transport.

The contribution made to crater volume by elastic volume transport is the main subject of this report. Further, we consider throughout only craters to which throwout contributes nothing, a simple limit suggested by DNA's PEACE exploration of Pacific craters (which stimulated this work)(Wardlaw, 1987).

The report's next section establishes elastic volume transport as a major cratering mechanism. Then, drawing as needed on knowledge of compaction, flow and elastic deformation, and on exact fields of

motion in which one or more of these three processes occur, we calculate and tabulate fractions of total crater volume that might result from them in various media. The last fraction (that for elastic transport) runs from about $\frac{1}{6}$ to $\frac{1}{3}$, but our results are approximate; for *axisymmetric* fields in which all three mechanisms operate, the equations of continuum motion have so far defied exact solution.

SECTION 2
TRANSPORT OF VOLUME BY ELASTIC WAVES

2.1 ELEMENTARY FIELDS.

We recall first the case of a flat elastic halfspace uniformly loaded by a pressure pulse of finite duration. The well-known result: The surface receives a permanent downward displacement equal to the impulse delivered per unit area, divided by acoustic impedance (i.e., longitudinal wavespeed times density) – and *the initial and final densities of material are identical.* This result (no density change) comes about as follows: The volume through which the surface drops is equal precisely to the volume of material removed by compression in the wave traveling downward through the medium. Thus, on asking where the volume of this "crater" lies, we find it moving down endlessly at constant speed, ever farther from the "cratered" (depressed) surface.

Turning next to the case of a spherical cavity in a homogeneous isotropic elastic wholespace, with pressure acting uniformly over the cavity wall, let that pressure grow to some new fixed value. The cavity radius then grows too. When the system stabilizes at the new cavity pressure, however, the density throughout the medium is again identical to its initial value. As in the case of the flat halfspace, a load impressed on the medium's surface produces no net change in volume strain; once more, a cavity-volume increase is made possible by compression in a wave that runs away from the cavity at constant speed, forever. Nor does similarity to the halfspace field end there: Below a plane through the center of symmetry, the added "crater" volume (half the change in cavity volume) is again proportional to the impulse that the pressure change delivers (to the medium) through that plane. The impulse in question remains finite, be it noted, even though the pressure change lasts for all time at the wall. [Physically: A vessel can confine fluid during and after a pressure buildup because tensile stresses develop in vessel material; on either side of a cross-sectional plane, the tensile force in the material offsets the force on the vessel due to fluid pressure, with the sum of the forces becoming zero at equilibrium. In holding cavity pressure forever, the wholespace acts like a vessel with very thick walls: In planar cross-section through the cavity's center, tractions in the material are indeed tensile (and normal to the plane).] These results, elementary but seldom brought up, are derived in Appendix A.

Linear elasticity, however, does not approximate well the behavior of material near the craters that explosions produce. Indeed, it does not allow permanent craters to form; as unloading proceeds, the ground surface regains its pre-shot shape. True, in a wholespace, permanent pressure in the cavity would leave it permanently enlarged, but (as big-hole decoupling demonstrates) by a small fraction of

the volume that an actual explosion produces. Rather, craterologists have invoked the inelastic processes of flow and compaction, mainly, to account both for permanent cratering and the growth of cavities in deeply buried bursts. Compaction aside, in an elastic-plastic medium, material deforms for a while at the maximum shear stress it can sustain (i.e., it inhabits states of shear failure), but with mean stresses of much higher amplitude; it deforms, therefore, almost in fluid (i.e., hydrostatic) states of stress – it flows. Even in a wholespace, however, stress levels decay with distance from shot-point (and, near the cavity, with time; cavity pressure drops as it expands); hence, shear failure does not occur beyond some finite distance (the "elastic-plastic" radius). Outward motion of the spherical shell of material at that radius increases the volume contained within it, and hence adds to the cavity's volume. Moreover, since deformation is elastic at all larger radii, that added volume again resides in material compression in an elastic wave, ever more remote, that moves outward at constant speed. At any given distance of propagation, however, the amplitude of the wave is enhanced (often greatly) by the incidence of shear failure within the elastic-plastic radius – one major aspect (among several that we discuss) in which cavity growth and crater growth are closely related. Next, therefore, we recall in more detail what goes on near the cavity, and add compaction to the combined effects of flow and elasticity.

2.2 PRINCIPAL STRESS, SHEAR STRESS, AND SPHERICAL MOTION.

The detonation front in a conventional explosion is, ideally, a sharp shock, and can be treated as such for most weapons effects purposes (by far); the same is then true (almost always) of the wavefront driven outward in adjacent material. In a nuclear burst, radiation-hydrodynamic interaction may occur at first between explosive and medium, but a sharp shock nonetheless develops in adjacent material, and soon (on the scale of crater or cavity size). In isotropic material, the shock causes straining only along its direction of travel ("uniaxial strain"). Strain in that direction is a principal strain, as are the null "lateral" strains in directions orthogonal to the shock. The corresponding components of stress (normal stresses) are also principal values, but (with rare exceptions) lateral *stresses* do not equal zero. In fact, all measurements say that lateral stresses can be as large as axial stress (fluids), but are smaller in solids; i.e., the pressure applied to the ends of a solid cylinder to compress it axially exceeds the pressure that must then be applied to keep it from expanding radially.

The directions in which principal stresses act – principal stress "axes" – are special in that, on a plane normal to any given axis, shear stresses vanish; across that plane, the force on material (per unit area: "traction") is axis-directed (i.e., normal to the plane). Across any other plane (neither parallel nor orthogonal to the shock direction, in the present instance) tangential components of traction (shear stresses) are linear combinations of differences between principal stresses. Hence, if all principal-stress

differences vanish (principal stresses equal, as in a fluid), then so do shear stresses (as in a fluid) – and the reverse also holds. Further, since there is a finite limit to the size of the shear stress that can develop in any real material, its principal-stress differences are also limited in size (at the limit or not, half of the largest difference between a pair of principal stresses equals the largest shear traction found on all planes through a given spatial point). Less formally put, matter does not have the "strength" to develop larger shear stresses or principal-stress differences than this material-specific limit allows; driven to its limit, it deforms ("flows") instead, without limit.

Principal stresses, being normal components of traction, can change during shear failure, but with the largest principal-stress difference fixed. Hence, in spherical fields, two of whose principal stresses are always equal, a change in any one of them must result in the same change in the other two during shear failure (the mean of the squares of their differences must not change). With shear stress at its limit, *changes in stress* are thus isotropic, precisely as they are in a fluid. Above the level that suffices to generate that limit at the cavity wall, pressure on the wall therefore tends (as in a fluid) to be imparted to the entire region of limiting stress, or "shear-failure" region (a region enlarged by the field's dynamics). Intuitively, such an outward projection of wall pressure should increase the displacement of surrounding material, adding to cavity growth. Strong support is lent to that notion simply by examining the equation (from mass and momentum conservation; Hopkins, 1960) that governs spherical-fields-in-general (whether elastic or not), namely

$$\rho a_r = -[\partial\sigma_r/\partial r + (2/r)(\sigma_r - \sigma_\theta)] \tag{2.1}$$

where ρ and a_r are the density and radial acceleration, respectively, of material at a point of radius r from the center of spherical symmetry; σ_r and σ_θ are the radial and hoop components of stress at that point, respectively (each being a principal stress, and *positive in compression*).

Specifically, in the outgoing shock from an explosion, stress in the direction of the shock (a principal stress; above) becomes radial stress; the lateral principal stresses – hoop stresses – are equal. Thus, σ_r starts out compressive and hence positive, and $\sigma_\theta \leq \sigma_r$ (above), so that $(\sigma_r - \sigma_\theta)$ is at first ≥ 0. Plainly [Equation (2.1)], the larger the value of the principal-stress difference $(\sigma_r - \sigma_\theta)$, the smaller the radial acceleration of just-shocked material. A limit to the size of shear stress, which now becomes a limit on $\frac{1}{2}|\sigma_r - \sigma_\theta|$ (above), therefore acts to increase the radial acceleration of that material. In elastic media, $\partial\sigma_r/\partial r$ (like wall pressure and σ_r) is also positive at and near the shock (σ_r falls on moving inward from it; Cooper, 1966); by enhancing outward transmission of wall pressure, shear failure causes $\partial\sigma_r/\partial r$ to decrease, and therefore again acts to increase a_r.

Note too that as just-shocked material moves outward, its hoop strains (both equal) become more

tensile (circles of particles about the center of symmetry expand). Its radial strain, however, tends to become more compressive; if a thin spherical shell of material were to move outward at constant volume, its rate of change of radial strain would be compressive and twice as large as that of hoop strain. Indeed, for radial strain ϵ_r to be expansive at a *greater rate* than hoop strain ϵ_θ, volume strain would have to grow at more than three times the rate of hoop strain. Until this last condition is reached ($-\dot{\epsilon}_r > -\dot{\epsilon}_\theta$, where $\dot{}$ signifies time-rate-of-change in a material element), σ_r in a real material may not decrease faster than σ_θ. In isotropic linear elastic media (as it happens) $-\dot{\sigma}_r > -\dot{\sigma}_\theta$ (hence $\dot{\sigma}_r - \dot{\sigma}_\theta < 0$) *if and only if* $-\dot{\epsilon}_r > -\dot{\epsilon}_\theta$. This need not be so for other substances; e.g., given shock-initiated shear failure, $-\dot{\sigma}_r$ can at least equal $-\dot{\sigma}_\theta$ during the period of flow in which $-\dot{\epsilon}_r < -\dot{\epsilon}_\theta$. Yet, the later stage of spherical motion in which $-\dot{\epsilon}_r > -\dot{\epsilon}_\theta$, is reached sooner without shear failure overriding linear elasticity. That is, by admitting large positive values of $\sigma_r - \sigma_\theta$ in the shock state, linear elastic behavior brakes a medium's outward motion, thus increasing $\dot{\epsilon}_\theta$ (making it less tensile) and reducing $\dot{\epsilon}_r$, and so gives rise more readily to the condition $-\dot{\epsilon}_r > -\dot{\epsilon}_\theta$. Reaching it ($-\dot{\epsilon}_r > -\dot{\epsilon}_\theta$) sooner during elastic deformation than during flow thus goes hand in hand with less cavity growth in the elastic case.

Stated in other (more common) terms: For a wide class of materials, increments in shear stress are proportional to shear-strain increments. The ratio of the former to the latter defines a shear modulus G that generally depends on the stress-strain state from which the increment occurs, and may depend on an element's entire stress-strain history in reaching that state (although for linear elastic materials, G is constant). G measures the material's resistance to shear deformation; the larger the value of G, the greater the shear-stress increment required to produce a given increment of shear-strain. And, during shear failure, G can be zero (Appendix B). With the shock at a given radius, however, a larger cavity implies larger values of ϵ_r and $-\epsilon_\theta$ (on average over disturbed material), and hence a larger shear strain [of magnitude $\frac{1}{2}|\epsilon_r - \epsilon_\theta|$ in spherical fields] – an increase unopposed by resistance to more shear when G=0, and resisted more and more strongly for larger and larger G. Small values of G go hand in hand with prodigious cavity growth.

2.3 DISPLACEMENT AROUND SPHERICAL CAVITIES: LINEAR ELASTICITY AND QUASISTATIC ELASTO-PLASTICITY.

Linear elastic media can have a wide range of G-values even if they have the same density ρ and longitudinal (radial) wavespeed c_p (hence impedance ρc_p and constrained modulus $M=\rho c_p^2$). They can therefore furnish a quantitative sense of the dependence of cavity growth on G. In particular, if the cavity pressure jumps suddenly to a constant level P beyond overburden (i.e., beyond mean stress in undisturbed material), then, after motion stops, the wall will have been displaced outward, relative to the cavity's radius for P=0, by a fraction $\frac{1}{4}P/G$ of that radius [Appendix A, Equation (A.11)]. Thus, as $G \to 0$ [elastic fluid; Poisson's ratio (ν)=$\frac{1}{2}$], the cavity grows without limit (a correct conclusion, even

though the linearization employed in reaching it is acceptable only if $\frac{1}{4}$P/G<<1). Moreover, as the field of motion develops, $\dot{\sigma}_r - \dot{\sigma}_\theta$ is positive in just-shocked material until the shock has traveled $\frac{3}{4}$M/G−1 initial cavity radii. At the cavity wall, which oscillates about its final radius, $\dot{\sigma}_r - \dot{\sigma}_\theta$ remains >0 for a time-interval determined (in units of the time taken by the shock to travel one cavity radius) by G/M alone, and hence on ν alone; that interval never ends when ν=$\frac{1}{2}$ (G=0), but decreases monotonically to 2.03 units of time at ν=$\frac{1}{4}$ and $\frac{\pi}{2}$ units at ν=0 (G=$\frac{1}{2}$M). Elastic or not, the shock-state with which an element's motion begins has $\sigma_r - \sigma_\theta \geq 0$, and $\sigma_r - \sigma_\theta$ starts to decrease when $-\dot{\sigma}_r > -\dot{\sigma}_\theta$; if linear elasticity holds up to a given "shock stress" (the value of σ_r in the shock state), then $\sigma_r - \sigma_\theta$ in just-shocked material approaches zero in the elastic-fluid limit [ν(Poisson's ratio)=$\frac{1}{2}$], and increases steadily to σ_r itself as ν decreases to zero.

Insight is gained more directly into the effects of flow on cavity size by considering quasistatic buildup of cavity pressure in a homogeneous isotropic medium whose shear-stress amplitude cannot exceed a fixed constant limit (von Mises limit), but is otherwise linear-elastic. For spherical fields, said limit on shear stress is evidently (above) equivalent to the constraint $|\sigma_r - \sigma_\theta| \leq$ Y, where the "strength" Y is a material-specific constant. In this case, the known exact field (Hill, 1956, p. 98-102) makes P/Y critical to determining the wall's outward displacement. For one thing, shear failure occurs around the cavity if and only if P>$\frac{2}{3}$Y. Then (for example), with ν=$\frac{1}{4}$ and K/Y=50 (K ≡ bulk modulus= M−$\frac{4}{3}$G), pressurizing the cavity causes its radius to increase by a factor of $\frac{5}{4}$ if P/Y=2.06, and a factor of 2 if P/Y=2.61; with K/Y=500 (and ν=$\frac{1}{4}$), cavity radius increases by factors of $\frac{5}{4}$ and 2 for P/Y-values of 3.49 and 4.09, respectively.

Of particular interest in these cases (ν=$\frac{1}{4}$ and K/Y-values of 50 and 500) is the source of the eightfold volume increase that occurs when the radius doubles – an addition to initial cavity volume V_o of $7 \times V_o$: With K/Y=50, material fails in shear out to 5.25 initial cavity radii, a boundary at which the outward displacement of material opens up a volume of $2.925 \times V_o$; the same outward transmission of cavity pressure (due to fluid-like behavior of failing material) responsible for that displacement also compresses failed material, shrinking the volume it occupies by $4.075 \times V_o$. For K/Y=500, the volume ($7 \times V_o$) added to the initial cavity has components $2.71 \times V_o$ due to outward displacement of material at the elastic-plastic boundary (initially at 11.06 radii) and $4.29 \times V_o$ due to compression of failed material. The profound effect of shear failure on cavity volume can be seen by considering buildups of cavity pressure identical to these, but with the medium strong enough (yet otherwise identical) to preclude shear failure at those pressures (Y ≥ $\frac{3}{2}$P). In the resulting purely elastic fields, outward displacement of the same material shells (initially at 5.25 and 11.06 cavity radii) open up volumes that equal just $.070 \times V_o$ (for P/K=2.61/50) and $.010 \times V_o$ (P/K=4.09/500). Moreover, except for nonlinear effects (very small here) of finite displacement, volume strains are zero in spherical-elastic fields around

cavities; compression of surrounding material adds nothing to cavity volume. And thereby hangs another tale of central importance later in this report: As already noted (Section 2.1), the medium's stress (hoop stress, σ_θ) is tensile over a plane through the center of the cavity if the medium is elastic; when shear failure occurs, however, σ_θ is compressive over the inner $\exp(-\frac{1}{6})$ (=.846) of the distance to the elastic-plastic boundary.

Subsequent quasistatic removal of pressure from the cavity wall ("unloading") raises further basic points. First, the wall will surely move inward as the pressure on it drops. Near the wall, that makes ϵ_θ (hence σ_θ) less and and less tensile (more compressive) even as σ_r becomes less compressive, so that $\sigma_r - \sigma_\theta$ falls from the value Y which, prior to unloading, obtains over the shear-failure region. Unloading therefore starts as an elastic process, remaining so unless and until it proceeds so far that $\sigma_r - \sigma_\theta$ reaches the value –Y (shear resistance to inward displacement then does not increase on further unloading). In particular, material will fail in the latter stages of unloading if P>$\frac{4}{3}$Y, as in the two examples above (ν=$\frac{1}{4}$; cavity radius doubles; P/Y=2.61, 4.09). More significant, though, is the small displacement that attends purely elastic unloading, which, in one case (P/Y=2.61), continues until the pressure has dropped at the wall to less than half of P. At that point, the decrease in cavity radius amounts only to $2\frac{2}{3}$% of the growth that took place during flow (when shear-strain increases went unresisted). For, flow stops when shearing is resisted (*elastic* unloading); material "freezes." True, flow will occur on still further unloading, but that fact holds only minor interest here: In explosions, wall pressure drops a great deal as the cavity expands; eventually, cavity growth stems not from pressure on the wall but from the outward velocity already imparted to material around the cavity.

2.4 SPHERICAL CAVITIES: DYNAMIC EFFECTS IN ELASTO-PLASTIC MEDIA.

Indeed, far from being quasistatic, cavity formation in an explosion is largely a matter of wave propagation; as the process unfolds in *time*, it presents us with some key facts and phenomena that do not enter the quasistatic limit. In particular, in an explosion, the cavity reaches static equilibrium (apart from minor damped oscillations about its final state) in a time inversely proportional to the medium's longitudinal wavespeed; dome-salt, in which near-spherical free-field motion has probably been best measured, has a wavespeed of 4.2 km/sec, and cavities driven by tamped bursts therein stabilize within 4 ms/$T^{1/3}$. For the simple elasto-plastic material above (relevant for dome-salt), stabilization comes about as shear failure ceases to occur in material around the cavity – the result of decay of both cavity pressure and shock stress. Material there unloads elastically, regaining the capacity to resist the changes in shear strain whose earlier unopposed development (in states of shear failure, starting with the initial shock state itself) made large outward displacements possible: The

medium stops flowing (failing in shear); it "freezes" by turning elastic as stress levels drop, just as it does during quasistatic relief of cavity pressure (above).

Dynamically, of course, material is disturbed at that time only out to the shock's finite radius; on that region, radial and hoop stresses do not exhibit quasistatic profiles – except that, at the cavity wall, radial stress must equal cavity pressure at all times in both cases. More important, an appreciable fraction of the work done on the medium resides in its kinetic energy (zero quasistatically). As a result, material continues to move outward well after $-\dot{\sigma}_r$ first exceeds $-\dot{\sigma}_\theta$ (the start of elastic unloading), because of matter's inertial resistance to changes in velocity. Thus, the cavity at first expands beyond its ultimate (equilibrium) size. Then, having developed a finite inward velocity in returning to that size, it moves inward still further (inertia again); *that* gives rise to compressive hoop strains and stresses (relative to the equilibrium state) in near-cavity material, which therefore slows and reverses direction – etc. There thus ensues a series of nearly-free oscillations of the cavity wall (*nearly*; cavity gases affect it slightly), diminishing in amplitude because the waves it generates in the medium, even if elastic, carry energy away from the cavity.

The oscillations *are* in fact elastic unless unloading is so strong in the first of them that $\sigma_r - \sigma_\theta$ drops all the way from Y (in the states of shear-failure that start with the shock) to –Y; this possibility is explored in Appendix B (which treats the subject in more detail), not because it alters much the picture drawn here of cavity stabilization, but because it explains why locked-in stresses (which are compressive) are limited in amplitude to Y. The larger fact to grasp is that the changes in stress which cause near-cavity material to keep reversing direction are largely (often entirely) elastic, and so take place with far less radial displacement than shear failure visited on the material; material freezes when shear-failure stops (which happens just before it first reverses direction; Appendix B.4). The reason (again): In shear-failure states, the growth of shear strain is not resisted; in elastic states, it is.

2.5 SPHERICAL CAVITIES: COMPACTION.

Like flow, in which the work done to create non-recoverable (i.e., inelastic) shear strain is converted to heat, any inelastic decrease in volume during hydrostatic compression ("compaction") converts work to heat (mainly during collapse of pores). Likewise, in spherical fields during flow, reduced resistance to shearing permits greater-than-elastic radial compression at a given radial stress (Appendix B.2), and the loose packing of grains or blocks of solid that leads to compaction (or even loose molecule-packing prior to transitions to denser phases) also enhances radial compression at that stress (cavity pressure, not medium-properties, sets radial stress at first). Either way, enhanced radial compression hastens early cavity growth (under a given pressure, the softer the medium the faster it moves). But- whereas

stress is transferred outward from the cavity wall through material that *flows* (above), the wall's *motion* is projected outward through material that *compacts.*

The reason lies in the relatively large increase in wavespeed typical of compaction. That is, compacted material tends to be much stiffer in compression, and especially in subsequent expansion, than in its initial loose state. Wavelets that signal slowing of the wall can therefore traverse disturbed material while the outgoing shock (the limit of disturbance) moves just a small fraction of the cavity's radius. At the same time, great stiffness in compression/expansion means that when the wall's radius changes by a given fraction, the volume through which it moves is equaled, roughly, by the volume through which any spherical sheet of compacted material moves. That is, the whole region of compacted material tends to move as a spherical piston of growing mass: As the wall slows, it all slows.

By the same token, if any sheet of compacted material were to slow, so would the wall – and, *were it not for shear failure*, that would actually happen before the cavity could grow appreciably. For, conversion of the medium to stiff *elastic* material via compaction would entail rapidly increasing resistance to the shear-strain changes implicit in outward radial motion (Sections 2.2, 2.4; Appendix B.3). High porosity and high strength, however, are strange bedfellows. Moreover, material does harden (grow stronger) as it compacts, but only toward the strength it has when consolidated. Thus, accounting for the motion of compacted material, and hence of the wall, returns us to the elastic-plastic case (Sections 2.3 and 2.4) – and again material freezes just before it reverses direction, effectively stabilizing the cavity.

The main effects of compaction, then, are (a) to inject a second dissipative process into cavity formation, thereby causing more rapid decay of the shock, and (more important) (b) to enlarge the ratio of wavespeed in disturbed material to that of the shock. The latter matter has great practical import because it lends physical sense to the treatment of shocked material as rigid-plastic (i.e., incompressible, but with finite shear strength), while reserving to the undisturbed medium ordinary compressibility in shock loading – a locking solid with strength. This in turn has *practical* impact because the problem of spherical motion in such a medium, when driven by radius-dependent pressure at the cavity-wall (an arbitrarily specified pressure), has been solved exactly (Trulio, 1992) – even allowing strength to vary with mean stress (as it often does in compactible media).

SECTION 3

APPROACHES TO THE PROBLEM, AND THE ROUTE CHOSEN

3.1 CRATERS FROM CAVITIES.

Evidently, a rather detailed answer can be given to the question of how cavities form around contained explosions, but what has that to do with the *craters* that explosions produce? Well – the two are linked in a general way by the mechanisms of flow and compaction, which play a major role in the formation of both cavities and craters. Moreover, the linkage becomes specific and quantitative in that the field around a spherical cavity automatically presents us with an instance of ground-surface loading – one with important similarities to the loads imposed by surface bursts. In a spherical field around a cavity, the loading in question is that found in the medium on any plane – a horizontal plane $\mathcal{P}$, say – through the burst-point; the hemispherical portion of the cavity wall below $\mathcal{P}$ completes the surface, and the pressure exerted on it by cavity gases is clearly relevant to surface-burst loading of the ground. As noted above, however (Section 2.1), the hoop stress imposed in plane $\mathcal{P}$ on the medium would be tensile and hence qualitatively (i.e., grossly) different from surface-burst loading, *if the medium behaved elastically.*

The exact fields at our disposal are not limited to elasticity, though; they include shear failure and compaction, which is fortunate even for understanding cavity growth, since models incorporating those processes better represent geo-materials than does elasticity alone. And, in plane $\mathcal{P}$, hoop stress presents a quite different picture for elasto-plastic media than for elastic ones; even in *quasistatic* spherical fields (as also noted above; Section 2.3), hoop stress is compressive almost to the elastic-plastic boundary (85% of the way out). In locking solids (with or without compaction), it remains compressive to at least the elastic-plastic boundary (Section 4 plots it in specific cases). Moreover, the material freezes (above) when the outgoing shock reaches that boundary; i.e., since material beyond the boundary resists shear elastically, elements of material thereafter execute only damped displacement-oscillations of small amplitude about their final radii. Up to the time of freezing, a loading wave sweeps outward over plane $\mathcal{P}$ imposing compressive normal tractions thereon, while gaseous products of the explosion press on the wall of the expanding crater that these tractions produce (half the cavity of the contained-burst field whence the tractions come) – all in qualitative agreement with surface-burst loading.

The field below $\mathcal{P}$ also *differs* strikingly from that of a surface burst, by presenting such major simplifications as a hemispherical crater (not merely bowl-shaped) and a just-sonic blast wave; noteworthy too is a discontinuity in loading pressure of amount Y [for simple materials (Appendix B.1)

during flow] on moving, at the crater's edge, from the crater-wall (vertical) to flat ground (horizontal). Yet, the surface tractions are of the right *kind*: compressive, spreading and diminishing in amplitude both with time and with distance from the burst point. The consequent fractions of crater volume due to compaction, flow and elastic volume-transport therefore warrant serious attention; they could prove representative of exact solutions for true surface bursts, and of the trends exhibited therein. Encouraging of such a prospect is the fact that (Trulio; 1984), for bursts at and near the flat surfaces of homogeneous halfspaces, motion is almost spherical in a cone of angle 60°, at least, that opens downward from its vertex directly above shot-point and grazes the crater's rim. Indeed, the present line of attack is less ambitious than attempts via "equivalent yield" (which the approach here resembles) to relate surface bursts to contained ones. That is, since the volume-fractions at issue are independent of yield, no absolute correspondence need be made between the two types of burst.

As to calculating the volume-fractions, some large points remain to be covered. The key: Given the state of the medium (out to the elastic-plastic boundary) after it freezes, we assume that almost the same state would have been reached had the medium's compressibility been at the low levels appropriate to elastic unloading after compaction. Pertinent compressibilities, where needed, come ultimately from lab measurements on materials of interest. Independently of those, but given that deformation is purely elastic outside the elastic-plastic boundary, the volume transported elastically to great distances equals that between the final and initial radii of material at that boundary (a spherical shell). Likewise, without reference to actual non-zero compressibilities, the exact locking-solid solution provides the volume compacted out of material between the cavity-wall and the elastic-plastic boundary. The third piece of the crater – the part added to its volume by flow – could be viewed as the volume transported elastically plus that taken up in compression by locked-in stresses (above). Having already accounted for the former, however, flow is associated here only with locked-in stress. The volume due to flow then follows from the mean-stress distribution out to the elastic-plastic boundary, using the medium's non-zero compressibility.

Finally, one takes account of a patent difference between surface and contained bursts, by unloading the ground surface to zero normal stress (.1 MPa, but who's counting). This last portion of the calculation, the only one that truly involves two spatial dimensions, has two parts. First, the cavity wall is relieved elastically of its uniform pressure by means of spherical deformation (by superposition, using the known field that results elastically from such relief), which alters the radial distribution of normal (hoop) stress over the flat part of the surface. The latter adjusted stresses are then relieved elastically, also by superposition, but using the known two-dimensional field produced by that relief (Love, 1944, p. 192). In the resultant field, the elastic-plastic boundary will have moved, becoming aspherical, and the volume between its former and new loci must be added to the prior estimate of the

volume transported elastically (or the entire calculation of said volume can await fixing the final locus). Similarly, the mean-stress distribution between the cavity wall (aspherical in the end) and elastic-plastic boundary will have changed too, requiring an addition to the prior estimate of volume-due-to-flow (or calculation of that volume from the final field).

3.2 RELATED EXACT FIELDS IN ELASTIC MEDIA AND INCOMPRESSIBLE FLUIDS.

The process outlined plainly provides no more than approximate final fields for surface bursts, and hence approximate crater-volume budgets for those axisymmetric fields (though the volume-fractions desired may well be more accurate than field-values at individual points). It does so, however, for media that deform inelastically, both hydrostatically and in shear, as well as elastically. No exact axisymmetric fields are known for such media. Rather, the roster of exact axisymmetric fields is limited to linear elastic materials, using linearized equations of motion, and to incompressible fluids. Those had been proposed nonetheless (for this program) as possible sources of estimates of elastic-transport volumes. One could learn, for example, where the volume of a dent goes when a localized load, impulsively delivered, is impressed on a linear elastic halfspace; as one item in question, permanent non-zero volume strains might develop near the loaded surface (if the load is not removed), or a part of that surface may be raised above its initial plane. Further, one would see how compression varies in the outgoing shock with direction from the central point of loading. At a more basic level, one might find that a local load, even though it delivers infinite impulse (if maintained indefinitely), will not displace the entire halfspace by a finite distance [the exact solution for quasistatic loading (loc. cit.) seems to imply that it will not]; if the local load is relieved, so that the impulse delivered is finite, then displacement of the entire halfspace does not seem possible [in the simple case of uniform loading (above), it takes infinite impulse to cause finite permanent displacement of the entire surface, so that finite impulse should impart no permanent displacement to it]. Moreover, questions like these would be answered for the quintessential simple *solid* – but at the price of a small-strain, small-displacement requirement that rules out indentations with crater-like shape.

On a halfspace of incompressible fluid, surface-burst loading would produce a crater which, under gravity, would eventually disappear. Without gravity, it might stabilize at finite size – but if so, would surely be huge relative to actual craters. That point aside, making room for the crater would call, in equal volume, either for a net outflow at great distances (across a vast spherical surface about the burst-point, say), or for the elevation of some or all of the medium's surface outside the crater; changes in material density are excluded by definition. The medium has charm nonetheless, because calculating exact flow-fields for it, *large strains and displacements included*, is a tractable problem (but not simple; solving Laplace's equation is the chief task). On the other hand, neither option (elastic

materials or incompressible fluids) permits compaction; further, flow too is excluded from elastic halfspaces, as is elastic deformation from incompressible fluids – each being a major omission from the mechanics of crater formation.

3.3 DISCRETE METHODS, AND THE APPROACH CHOSEN.

Massive computation based on discrete equations of motion – a favored option in the computer age – was relegated from the outset to no more than a supporting role (mainly to be played later, for purposes of comparison). To be sure, discrete methods have the advantage of readily admitting in a material the modes of behavior noted (and others, to the point of diminishing returns). The aim here, however, is to cover a wide range of those properties, and each choice of the set of them gives rise to a distinct cratering field. Calculating one such axisymmetric field is expensive, and the result becomes exact only in the limit of infinite expense. In practice, that is, discrete methods always give inexact answers to the specific problems of motion posed, and their cost is compounded when one seeks high accuracy at late times and/or large distances.

In particular, for axisymmetric fields, the number of arithmetic operations must grow as the cube of final problem time if we are to have much hope of controlling discretization error. Even then, error-control is less than certain: It has not been shown that discretization error *can* be kept in check as a cratering problem is run on and on, and to make such an evaluation with confidence would be expensive and time-consuming. Yet, for present purposes, a numerical field without a demonstrable *bound* (at least) on its error would be worthless. Likewise, so are such tricks as computing the near field using discrete cells of the usual size, and then equating the volume transported elastically to the final computed crater volume minus the sum of "permanent" volume changes over all cells of the discrete mesh. For one thing, without artificial damping (explicit or implicit in the discrete equations of motion), the mesh-nodes for such a problem oscillate indefinitely, and it is not known how much the final *axisymmetric* density field, damped, differs from the undamped one sought. The displacement of material at a discrete elastic-plastic boundary is subject as well to that uncertainty.

In sum: (i) Cost, of itself, sufficed to tip the scales against massive computation. (ii) Either course (heavy computing, or using exact solutions to *related* problems) yields only approximate results, but, with regard to understanding the defects of the crater-volume budgets obtained, clearcut physical compromises are much to be preferred to the obscure (and, mathematically, no less complex) effects of discretization error. Thus, early in the program, a choice had to be made between exact solutions that take account of just one of the three physical processes most basic to cratering, and *related* exact solutions which include all three. Given the objective of determining what these very processes might contribute to final crater volume, and almost no prior estimates thereof, we chose to employ model-

materials capable of flow, compaction and elastic deformation – and compromised on completeness and exactness in other aspects of the problem (chiefly ground loading and the passage from locked solids to stiff elastic ones). In short, the approach outlined in Section 3.1 was adopted.

SECTION 4

THE FIELDS CALCULATED: MEDIA, PROCEDURE, AND RESULTS

4.1 CONSTITUTIVE EQUATIONS.

In calculations, including those reported here, *models* define materials. The models take the form of equations ("constitutive equations") which, ultimately, relate stress and strain increments in any given element of material. Each such equation-set defines a class of substances. Individual members of the class are specified by the values assigned to all the arbitrary (within limits) constants contained in the equation-set (material properties "parameters"). Comprising the constitutive equations used in this work are: (i) a curve of stress vs. strain (uniaxial) for shock loading, from whose states *all* subsequent stress-strain changes take place at constant volume (reloading to higher mean stresses than in the initial shock, if that occurs, is then easy to handle); (ii) the requirement that, in shock-states, for which σ_r and σ_θ are denoted σ_r^s and σ_θ^s , $|\sigma_r - \sigma_\theta|$ equal the smaller of Y and $\sigma_r(1-2\nu)/(1-\nu)$, and that otherwise (iii) $|\sigma_r - \sigma_\theta|$ equal the smaller of Y and $|\sigma_r^s - \sigma_\theta^s - 6G\epsilon_\theta|$, with $\sigma_r - \sigma_\theta = \sigma_r^s - \sigma_\theta^s - 6G\epsilon_\theta$ when Y is the larger number. In calculating elastic transport of volume outward from the elastic-plastic boundary, material beyond the boundary obeys the equations of isotropic linear elasticity, which (in this context) reduce to $\sigma_r = \lambda\Delta + 2G\epsilon_r$ and $\sigma_\theta = \lambda\Delta + 2G\epsilon_\theta$, where $\Delta \equiv \epsilon_r + 2\epsilon_\theta$; the same equations are used to compute the elastic compression that locked-in stresses would cause. The model's parameters are then the constants Y, ν, G, λ, and those of the loading curve, for which two different algebraic forms were used: $\sigma_r^s/\sigma_o = (\epsilon_r^s/\epsilon_o)^\alpha$ ["power-law"] and $\sigma_r^s/\sigma_o = a(\epsilon_r^s/\epsilon_o) + b(\epsilon_r^s/\epsilon_o)^2 + b(\epsilon_r^s/\epsilon_o)^3$ ["cubic"], whose parameters σ_o, ϵ_o, α, a, b and c occur in just four independent combinations (one in the power-law equation for σ_r^s/σ_o and three in the cubic). Compared to most geo-material-models now in use, this one is quite simple, as befits an exploratory program of the present kind. An equation for pressure (radial stress) at the wall of the cavity completes these problems' specification; said pressure was made a function of cavity volume (hence radius) by means of accepted equations of state for detonation products (homogenized; Trulio 1992, Section 3.2).

The burden and results of the PEACE program having prompted this work, the parameters noted were assigned values derived mainly from lab tests of either Pacific coral or (lacking data for coral) limestone. Thus, in the four principal media for which volume budgets have been obtained under the subject contract, Y was set at 10 MPa – twice or thrice that actually measured for Pacific coral (Borschel, Klauber and Early, 1986, pp 81 & 93) because the present application spans several times the depth whence came the samples tested, and, deeper down, the medium may be stronger. Further, ν was assigned the value .21 (Borschel, Klauber and Early, 1986, p 129) in all four; in one of them, however, ν was also set to 0 (λ=0) and –1 (the lowest value possible elastically) with all other

parameters held fixed. Three of the media had power-law loading curves (with exponents 2, 8.4 and 1); the fourth (the one with which ν-values of .21, 0 and −1 were used) had a cubic curve of loading. At low stress levels, the latter curve fits uniaxial stress-strain data for Pacific coral (Blouin and Timian, 1986, p 124); it also fits selected stress-strain points well above the limit of those data (.17 GPa of axial stress), conforming roughly to Hugoniot measurements for Indiana limestone at 10 GPa (Murri, Grady and Mahrer, 1975). The loading curve so defined represents fairly well the data cited over the range of shock stress met with here: $0 \leq \sigma_r^s \leq 14.5$ GPa. The power-law curve with α=2 is a fit to the same lab-test data for axial stresses up to $\sim$.17 GPa (though used to much higher stresses). The curve with α=1 passes through the 10-GPa point, but is intended mainly to set a plausible minimum on energy dissipation in shock loading (zero) because the Rayleigh line and loading curve then coincide; α=8.4 comes close to maximizing such dissipation, besides which, with α=8.4, a close fit is obtained to the measurements of axial stress at 10 GPa (above), and to the highest-stress point ($\sim$.17 GPa) of one test in the set whose overall data suggested α=2. The constant σ_o is equal to the mean pressure of cavity gases when detonation ends (given a chemical-explosive sphere, tamped in the medium and center-detonated). Then, having specified α for a power-law loading curve, ϵ_o is obtained by forcing the curve to pass through a specific stress-strain point (at 10 GPa for α=1; .17 GPa for α=8.4 and 2); for the cubic, whose coefficients depend on the choice of ϵ_o, the value chosen for it forces their sum to equal 1 when σ_r^s=σ_o, and the curve must go through (σ_o,ϵ_o). Further, exclusive use of the explosive Composition C4 (as defined by a JWL equation of state; Lee and Finger, 1974) to drive the medium, led to the value 14.5 GPa for σ_o. In some respects, especially in the shape of the curve of uniaxial loading and the "Poisson's ratio" ν, a broad range of materials was covered by this pilot study; for others (Y in particular) its coverage was highly limited or minimal.

4.2 THE SPECIFIC PROBLEMS FOR WHICH EXACT SOLUTIONS WERE FOUND.

Table 4-1 below lists the combinations of parameter and loading-curve choices defining the media for which we computed crater-volume budgets. As explained above (Section 3), exact fields driven explosively into locking solids form the basis for the various budgets, and all the properties defining those solids appear in the table (each row thereof, and hence a solid, is labeled in the table's first column simply by the number of the locking-solid problem solved in evaluating, for that solid, the exact solution). The "Shear Modulus, G," listed in the last column, does not actually enter the exact locking-solid solution, however. True, once shocked, a thin spherical shell of material continues to fail in shear if and only if, on assuming its subsequent changes in strain to be elastic, one obtains principal-stress differences $\geq$ Y. Since all deformation takes place at *constant* volume-strain Δ (Section 4.1), this means that shear failure ($\sigma_r - \sigma_\theta$=Y; rigid plasticity) continues if and only if $|\sigma_r^s - \sigma_\theta^s - 6G\epsilon_\theta| \geq Y$ as the shock runs past the shell. Now, ϵ_θ is zero in just-shocked material because displacement cannot

Table 4-1. Parameters used in material models.

Problem Number	Loading Curve	ϵ_o	α	Poisson's Ratio, ν
9	Power-law	1.68939556	2.0	0. 21
10	Power-law	0.31368232	8.4	0. 21
11	Power-law	0.36361471	1.0	0. 21
12	Cubic	0.29678248	*	0. 21
12a	Cubic	0.29678248	*	0. 00
12b	Cubic	0.29678248	*	−1. 00

For all problems:

Explosive: Composition C4

σ_o: 14.5445838 GPa

Y: 10.0 MPa

G: 2.0 GPa

* Coefficents of cubic

a = .1081465913

b = .5664047702

c = .3254486385

jump in an instant. But, because the shock imparts outward velocity to the shell, ϵ_θ becomes increasingly tensile (<0) thereafter so that, with $\sigma_r^s - \sigma_\theta^s$ =Y, we find $\sigma_r^s - \sigma_\theta^s - 6G\epsilon_\theta > 0$ ($\sigma_r^s - \sigma_\theta^s - 6G\epsilon_\theta = \sigma_r - \sigma_\theta$ for rigid-*elastic* deformation). Hence, the shell continues to fail in shear. By the same token, if $\sigma_r^s - \sigma_\theta^s$ were to fall below Y beyond some radius (due, say, to decay of shock-stress levels as the shock moves outward), $\sigma_r - \sigma_\theta$ would return at once to the value Y. Thus, by driving material outward, the shock also forces it to fail in shear; moreover, outward-moving material keeps on failing in shear. In turn, since compressive shock stress causes outward motion, the medium moves in shear-failure states until the shock's strength decays to zero – which, given shear failure, happens at a finite radius [Trulio, loc. cit.; cohesion (in this case Y) enters the shock stress equation as a direct reduction of cavity pressure because flow at fixed shear stress Y/2 need only occur in a finite mass in order to dissipate the explosive's finite energy].

To introduce elastic volume-transport into such an exact solution, the medium is treated as linear-elastic beyond an elastic-plastic boundary defined as follows: For each position of the shock (out to that boundary) the radial velocity of a just-shocked shell is known, and cannot jump discontinuously at any radius (because it would then have to jump throughout the mass of locked solid, which would take infinite force). If a shock were driven by locked solid into elastic material just beyond a given radius, the radial velocity found in the locked material just shocked would therefore be imparted to the adjacent elastic shell. Values having been assigned to that shell's elastic moduli and density, its longitudinal wavespeed is also known – and with it, radial stress in the shell's shock-state (the product of density, wavespeed and radial material velocity), hoop stress, and their difference $\sigma_r - \sigma_\theta$ [radial stress times $(1-2\nu)/(1-\nu)$, since the shock state is one of uniaxial strain]. The elastic-plastic boundary lies (before displacement develops there) at the radius for which $\sigma_r - \sigma_\theta$, so computed (i.e., *in the elastic shell)*, equals Y.

Since the moduli define a material much stiffer in compression than the loading curve requires (at low stresses), radial stress jumps to higher levels than in the shock (through locking solid) incident upon the boundary. That compressive jump is felt at once throughout locked solid as a similar radius-dependent jump (zero only at the cavity wall); velocity must be continuous, but not acceleration. Owing to the great stiffness of the elastic medium, particularly in shear, the system now freezes (Section 2.3). That is, small tensile changes in hoop strain (hence in radial displacement) cause relatively large tensile changes in hoop stress in the outgoing elastic wave, soon bringing outward motion of the elastic-plastic boundary to a halt, and the boundary starts to move inward. Now, however, hoop strain becomes more compressive in locked solid, causing $\sigma_r - \sigma_\theta$ to fall below Y, so that (finally) rigid-*elastic* deformation of locked material occurs; the large shear modulus for such deformation restricts the oscillation to virtually negligible displacements. The exact solution extends to

this spherical system as well: locking solid, elastic (in shear) and plastic, surrounded by an elastic medium. Volume transported elastically issues from it; a close approximation thereto comes from applying the shock stress incident on the elastic-plastic boundary to the outside elastic medium, as a quasistatic load.

In the shear-failure region, where larger compressive stresses are found than outside its elastic-plastic boundary, elastic moduli for unloading/reloading to vary with shock stress. Specifically, data from UX tests of Pacific coral show nearly elastic unloading/reloading from a given loading state, but with moduli M and G that depend appreciably on the loading state chosen (Borschel, Klauber and Early, loc. cit.). Nonetheless, G and the Poisson's ratio ν_u for unloading/reloading were assigned constant values (2 GPa and .21, respectively, found at the higher stresses of UX measurement); from the usual definitions of elastic moduli, G and ν_u imply a constrained modulus M, and also a bulk modulus K ($=M-\frac{4}{3}G$). For a given spherical shell of material, the locked-in elastic volume-strain (the change in its volume-strain that would occur on unloading to overburden) equals its locked-in mean stress $\overline{\sigma}$ $[=\frac{1}{3}(\sigma_r+2\sigma_\theta)]$, divided by K; thus, the product of $\overline{\sigma}/K$ with the shell's final volume gives its contribution to locked-in volume. Summing over all shells in the shear failure region [i.e., evaluating $\int(\overline{\sigma}/K)4\pi r^2\,dr$ across the shear-failure region], we obtain the total volume locked into that region – the contribution of flow to the crater's volume.

Formulas for the change in the field due to unloading of the ground surface are those of strict linear isotropic elasticity, and hence contain just two constant moduli (bulk and shear moduli, say). Long since published (Love, loc. cit.), they yield the following expressions for the vertical (u_z) and horizontal-radial (u_R) components of displacement at an arbitrary vector-position $\underline{r}$ in the halfspace:

$$4\pi G u_z = 2(1-\nu)\phi - z\partial\phi/\partial z \quad ; \quad \phi \equiv \int\int_{GS} \sigma_n(x',y')\,\frac{dx'dy'}{|\underline{r}-\underline{r}'|} \tag{4.1}$$

$$4\pi G u_R = -z\partial\phi/\partial R - (1-2\nu)\partial\chi/\partial R \quad ; \quad \partial\chi/\partial R \equiv \int\int_{GS} \frac{\sigma_n(x',y')[R-R'\mathrm{Cos}(\varphi-\varphi')]}{|\underline{r}-\underline{r}'|(z+|\underline{r}-\underline{r}'|)}\,dx'dy' \tag{4.2}$$

where integration extends over the part of the ground-surface plane [the (x,y)-plane of a Cartesian (x,y,z) frame] loaded with non-zero normal stress $\sigma_n(x,y)$ (hoop stress in the exact spherical solution, after unloading the cavity wall; Section 2.1); also, z denotes vertical position, increasing with depth, x',y',0 are the position-components of an arbitrary point on the ground-plane. Points $\underline{r}$ and $\underline{r}'$ have cylindrical coordinates R,φ and R',φ' (x=R Cosφ, y=R Sinφ; x'=R'Cosφ', y'=R'Sinφ'). Here $\sigma_n(x',y')$, a function only of R', is the normal stress at $\underline{r}'$ when the medium freezes, so that the region GS becomes the circle (about shot-point) whose radius equals the elastic-plastic radius r_{ep}; passage to

cylindrical coordinates is therefore convenient, whereupon $R'dR'd\varphi'$ replaces $dx'dy'$, $0 \leq R' \leq r_{ep}$ and $0 \leq \varphi' \leq 2\pi$, and ϕ and $\partial\chi/\partial R$ (hence u_z and u_R) are independent of φ [also, $|\underline{r}-\underline{r}'|^2=z^2+R^2+R'^2-2RR'Cos(\varphi-\varphi')$].

4.3 RESULTS.

At about the time it freezes in our exact spherical field, medium 12 (a locking solid with strength; Table 4-1) exhibits the hoop-stress distribution plotted as a function of radius in Figure 4-1. That stress (as it evolves with time), if imposed normally on a flat halfspace of the same material (except for a hemispherical indentation loaded with the cavity's pressure), produces every detail of the field found spherically. As a ground-surface load, it is therefore compared in the figure with two others that come, respectively, from computer simulations of conventional and nuclear surface bursts (zero height-of-burst) – the Middle Gust 4 event (Ito, 1995) and an unspecified one (Brode, 1964) Since no known scaling law relates the three fields, the general idea of crater-volume scaling (Cooper, 1976) was employed in selecting the overpressure profiles shown. Specifically, the profiles are found in each of the two latter fields at about the time when the loading wave has moved outward by the number of cavity radii seen in the hoop-stress profile [the cube of cavity radius at a given time being defined as then-current cavity-volume $\times (.75/\pi)$]. Further, differences among the three media were taken into account at the outset by applying to current crater volume a crude empirical factor that allows crater size to vary with medium (soil, soft rock and hard rock; Cooper, 1976).

The shapes of the surface-burst profiles are plainly much more alike than either is to the hoop-stress profile, displaying peak values not near the crater but farthest away from it (i.e., at the front of the loading wave). That fact evidences the different physical objects – airblast front vs. locked-in stress – presented by the two types of peak. Peak loading stresses are about 7 times as large in medium 12 as for the surface bursts, and, in the more important matter of vertical force exerted on the ground, the ratio is ~ 10 – but, at the wavefront, the stress-ratio is $<\frac{3}{2}$. Thus, the two types of ground-loading might give rise to similar crater-volume contributions, percentagewise, from elastic transport. The higher stresses in medium 12, however, argue that the present fields overstate the contribution to crater volume from compression, elastic or not. To answer such questions requires a better match to surface-burst loading than is provided by the hoop-stress profiles from contained bursts. Such improvement can result from varying the cavity-radius/wall-pressure relation by which our exact fields are driven. The exact solution offers great leeway in setting that relation, which was in fact varied for medium 12 to produce the more satisfactory match to surface-burst loading seen at the bottom of Figure 4-1; to obtain the hoop-stress curve shown there required dictating far more rapid decay of cavity-wall pressure than that due to cavity gases in a contained burst – aping, crudely, the expansion

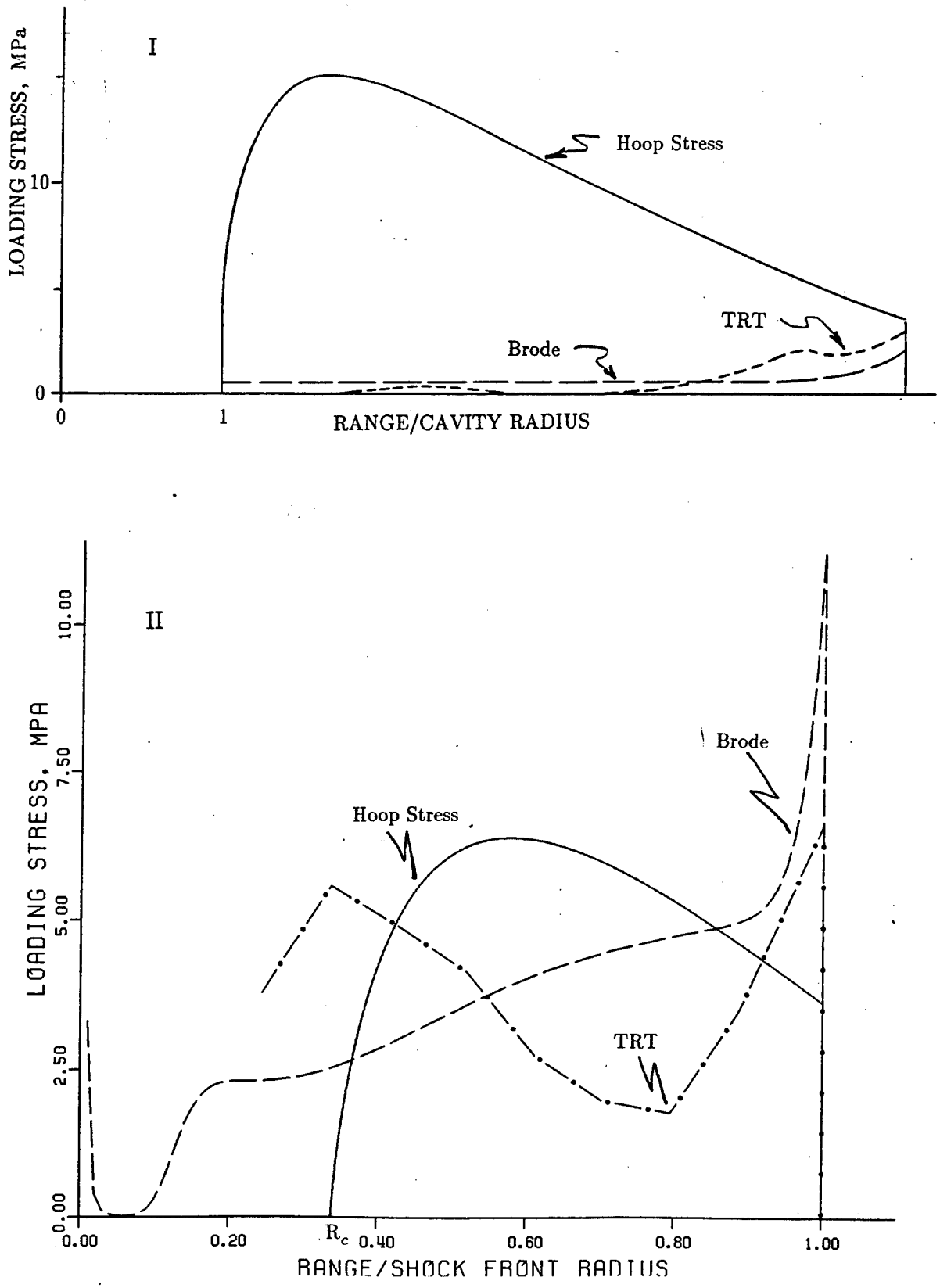

Figure 4-1. Comparison of normal stress loads on the ground surface from: This paper [Hoop Stress (Medium 12)], a nuclear surface burst (Brode) and a conventional burst (TRT). For graph I, the pressure of gaseous detonation products drives the field whose Hoop Stress is plotted. Graph II employs a faster-falling relation between cavity pressure and radius, contrived to make Hoop Stress match more closely the TRT and Brode ground-surface loads.

of gaseous detonation products into the atmosphere during surface bursts.

As for the three contributions themselves (locked-in elastic volume, elastic transport and compaction), Table 4-2 lists the fractions of final crater volume due to each, for the six media of Table 4-1. The fraction due to elastic transport ranges from about $\frac{1}{6}$ to $\frac{1}{3}$, a fairly narrow range considering the large variations in shock-loading-curve and Poisson's ratio covered by these media (but Y, probably at least as important a material property in determining the volume-fractions of Table 4-2, was not varied). Most sensitive to changes in the medium's properties is the portion of crater-volume due to its elastic compression by locked-in stresses; this volume-fraction runs from barely significant ($\sim \frac{1}{25}$) to substantial ($\sim \frac{1}{4}$). Further, since the boundary condition at the crater-wall is one of specified pressure P, and the parameter P/Y dominates quasistatic cavity formation, the volume-fractions at issue might span a much wider range if Y were varied. As matters stand, the compaction-fraction is largest in all cases (running from .44 to .80). Given the program's variety of shock-loading curves (of power-law type especially), that result was not foreseen; e.g., with σ_r^s/σ_o=.1, the fraction ϵ_r^s by which volume irreversibly decreases via shocking is given by ϵ_r^s/ϵ_o=.1 when α=1, and ϵ_r^s/ϵ_o=.76 when α=8.4. A possible explanation: Each of our loading curves admits so much compaction that even for the least compactible medium of the lot (α=1), compaction must account for a large part of the space made available for cavity expansion. High-porosity Pacific coral, after all, was the medium whose measured properties most influenced the sets of parameters for which our exact field was evaluated. Indeed, in *retro*spect, one might have wished for less emphasis on the Pacific and more on diversity of media. *Pro*spectively, more relevant halfspace loadings such as that at the bottom of Figure 4-1 [even if found in spherical fields by discrete methods (fine zoning)], should be used to assess the accuracy of the accounts of cratering that massive computation yields.

Notwithstanding the restriction to just one Y-value, insensitivity of the crater-volume budget in medium 12 to a drastic change in pressure at the cavity wall (part II of Table 4-2), and to the simulated ground-surface loading that follows from wall-pressure (Figure 4-1), must be counted a major result of this study. In particular, the fraction of crater volume that resulted from elastic transport – the study's main concern – changed from .33 to .29. More strongly affected was the volume-fraction due to residual compression, which dropped from .22 to .14 – a direction of change consistent with the much-enhanced decay of wall-pressure that caused it. The two reductions noted entail an increase from .45 to .57 in the compaction-fraction, because the contributions made to crater volume by elastic relief of pressure on the hemispherical crater, and on the ground-surface plane, proved negligible. Relief of cavity-wall-pressure, for example, made a change of only .15% in the volume swept out by the elastic-plastic boundary (i.e., in the volume transported elastically to remote regions). This was so despite the large pressure, relative to that in a surface-burst crater, remaining at

Table 4-2. Fractions of final crater volume contributed by elastic transport, compaction and residual elastic compression arising from flow. The fields of part I were driven by the pressure of gaseous detonation products. Part II employs a faster-falling relation between cavity pressure and radius, contrived to make Hoop Stress match more closely the TRT and Brode ground-surface loads.

	Medium	Residual Compression	Elastic Transport	Compaction
I	9	.15	.31	.54
	10	.04	.16	.80
	11	.26	.30	.44
	12	.22	.33	.45
	12a	.20	.33	.47
	12b	.17	.32	.51
II	12	.14	.29	.57

the cavity wall when the outgoing shock reached radius r_{ep} – a shortcoming of the present cratering model [to keep hoop-stress positive meant that radial stress (wall pressure) could be no smaller than Y (10 MPa here)]. Yet, the negligible effects of surface stress-relief also confirm a cornerstone of the model: When shear failure stops, so does crater growth; the medium around the crater does indeed "freeze" at that time.

SECTION 5
REFERENCES

Blouin, S. and Timian, D., 1986, *Material Properties Testing in Support of PEACE Program, Enewetak Atoll* , ARA Report No. 5958, Applied Research Associates, Inc., South Royalton, VT, (UNCLASSIFIED).

Borschel, T., Klauber, W. and Earley, K., 1986, *Lithologic, Physical and Mechanical Characterization of Geologic Samples from Enewetak Atoll*, DNA-TR-87-40, Terra Tek, Inc., Salt Lake City, UT, (UNCLASSIFIED).

Brode, H., 1964, *A Review of Nuclear Explosion Phenomena Pertinent to Protective Construction,* Rand Report No. R-425-PR, The Rand Corporation, Santa Monica, CA, (UNCLASSIFIED).

Cooper, H., 1966, *Generation of an Elastic Wave by Quasi-static Isentropic Expansion of a Gas in a Spherical Cavity; Comparison between Finite Difference Predictions and the Exact Solution,* AFWL-TR-66-83, Air Force Weapons Laboratory, Kirtland Air Force Base, NM, (UNCLASSIFIED).

Cooper, H., 1976, *Estimates of Crater Dimensions for Near-Surface Explosions of Nuclear and High-Explosive Sources*, RDA-TR-2604-001, R&D Associates, Marina Del Rey, CA, (UNCLASSIFIED).

Courant R. and Friedrichs, K., 1948, *Supersonic Flow and Shock Waves*, Interscience Publishers, Inc., New York, NY, (UNCLASSIFIED).

Hopkins, H., 1960, *Dynamic Expansion of Spherical Cavities in Metals*, Progress in Solid Mechanics, Volume 1, Chapter III, p 137, North Holland Publishing Co., Amsterdam, Neth., (UNCLASSIFIED).

Hill, R., 1956, *The Mathematical Theory of Plasticity*, pp 98-102, Oxford at the Clarendon Press, London, Eng., (UNCLASSIFIED).

Ito, M., 1995, Facsimile dated 16 September to J. Workman of Applied Theory, Inc., Titan Research and Technology, Chatsworth, CA, (UNCLASSIFIED).

Landau, L. and Lifshitz, E., 1970, *Theory of Elasticity*, McGraw-Hill, Addison-Wesley Publishing Company, Inc. Reading, MA, (UNCLASSIFIED).

Lee, E. and Finger, M., 1974, Memorandum to D. Larson of Lawrence Livermore National Laboratory, Lawrence Livermore National Laboratory, Livermore, CA, (UNCLASSIFIED).

Love, A., 1944, *A Treatise on the Mathematical Theory of Elasticity*, p 192, Dover Publications, New York, NY, (UNCLASSIFIED).

Murri, W., Grady, D. and Mahrer, K., 1975, *Equation of State of Rocks,* Final Report Contract AT(04-3)-115, Stanford Research Institute, Menlo Park, CA, (UNCLASSIFIED).

Rawson, D. et al., 1966, *Post-Explosion Environment Resulting from the Salmon Event,* J. Geophys. Res., Vol. 71, No. 14, p 3510, (UNCLASSIFIED).

Rogers, L., 1966, *Free-Field Motion near a Nuclear Explosion in Salt: Project Salmon,* J. Geophys. Res., Vol. 71, No. 14, pp 3415-3426, (UNCLASSIFIED).

Stratton, J. A., 1941, *Electromagnetic Theory,* McGraw-Hill, New York, NY, (UNCLASSIFIED).

Trulio, J., 1984, *Strain-Path Modeling for Geo-Materials,* DNA-TR-84-105, Applied Theory, Inc., Los Angeles, CA, (UNCLASSIFIED).

Trulio, J., 1992, *Ground Shock Studies for Shallow Buried Explosions: Volume II—Spherical Fields in Locking Solids,* DNA-TR-91-175-V2, Applied Theory, Inc., Los Angeles, CA, (UNCLASSIFIED).

Wardlaw, B., 1987, *Integration of Material-Property Units, Gravimetry, and Additional studies of Oak and Koa Craters,* Pacific Enewetak Atoll Crater Exploration (PEACE) Program, Enewetak Atoll, Republic of the Marshall Islands, Part 4: Analysis of borehole gravity surveys and other geologic and bathymetric studies in vicinity of OAK and KOA craters, Chapter 7, U. S. Geological Survey Open-File Report 87-665, (UNCLASSIFIED).

APPENDIX A

LINEAR ELASTICITY: IMPULSE AND SPHERICAL CAVITY GROWTH

In the usual limit of small strain and displacement, motion is governed in linear elastic isotropic media by two wave equations, one for the irrotational part of material displacement (or velocity), and the other for its solenoidal part (Landau and Lifshitz, 1970). The former's waves move with longitudinal speed, while those of the latter equation move with transverse speed. In homogeneous isotropic wholespaces, however, spherical fields of motion are produced when pressure is applied uniformly to the walls of spherical cavities. Material displacement (or velocity) is then radially directed and, like all properties of spherical fields, varies only with radius (measured, in this case, from the center of the cavity). Such displacement (or velocity) fields are curl-free – i.e., irrotational (Courant and Freidrichs, 1948). As a result, material displacement (or velocity) equals its irrotational part, and so satisfies a wave equation with longitudinal wavespeed. Moreover, since material moves on radial lines, and displacement (or velocity) varies only with radius and time, we need only express the displacement vector and the LaPlacian ∇^2 in spherical coordinates (Stratton, 1941) to find from the wave equation that

$$c_p^{-2}\partial^2 u_r/\partial t^2 = r^{-2}(\partial/\partial r)(r^2\partial u_r/\partial r) - 2r^{-2}u_r \qquad (A.1)$$

where t, r, u_r and c_p denote time, radius, radial material displacement (or velocity) and longitudinal wavespeed, respectively. Any given plane $\mathcal{P}$ through the center of the cavity is orthogonal to all spheres about that center, and can therefore be taken as the surface on which the spherical coordinate θ is equal to $\pi/2$. The stress component σ_θ normal to $\mathcal{P}$ is a principal stress (hoop stress) – and, by definition, compressive stress is taken as positive herein. If the cavity wall, whose radius is a, is subjected impulsively to pressure P at time t=0 – a pressure held fixed thereafter – then Equation (A.1) implies the following on $\mathcal{P}$ (Cooper with γ=0):

$$\sigma_\theta \equiv \sigma_\theta(\xi,\tau) = (-\tfrac{1}{2}P/\xi^3)\{1 - [(1+2\beta\xi^2)\mathrm{Cos}(\kappa\zeta\delta) + (1-2\xi-2\beta\xi^2)\tfrac{1}{\delta}\mathrm{Sin}(\kappa\zeta\delta)]\ \exp(-\kappa\zeta)\} \qquad (A.2)$$

Equation (A.2) holds for $t \geq 0$ and $0 \leq r-a \leq c_p t$, while σ_θ=0 if $r-a > c_p t$. For $r \leq a$ and $t \geq 0$ we obtain σ_θ=P (on $\mathcal{P}$) by considering the cavity to be full of gas at pressure P [the force over the circle subtended on $\mathcal{P}$ by the cavity is thus normal to $\mathcal{P}$ with magnitude $\pi a^2 P$; more rigorously, one obtains the same result for the force on the hemispherical cavity surface below $\mathcal{P}$, by summing (over that surface) the tractions $P\underline{n}_w$ at all its points ($\underline{n}_w \equiv$ unit outer normal at a given point)]. Also, the state of zero stress (for P as well as in the medium) is that of the medium infinitely far from the cavity (assumed hydrostatic). Further, the variable ζ denotes $\tau-\xi+1$, where the nondimensional time τ and radius ξ equal, respectively, $c_p t/a$ and r/a; for the solid with shear modulus G and constrained modulus M, the constants β, κ and δ equal 1–2G/M, M/G and $(-1+M/G)^{1/2}$, respectively. We note

too that $M=\rho c_p^2$ (where ρ is the material's density), and that $2G/M=(1-2\nu)/(1-\nu)$ if ν denotes Poisson's ratio.

The force acting on $\mathcal{P}$ is normally directed (vertically downward, say); the amplitude of the force is given by

$$F(t)= \int_0^{a(1+\tau)} \sigma_\theta 2\pi r dr = 2\pi a^2 \int_0^{1+\tau} \sigma_\theta \xi d\xi = \pi a^2 P - \pi a^2 P \left\{ \int_1^{1+\tau} d\xi/\xi^2 - \int_1^{1+\tau} \psi(\xi,\zeta)\exp(-\kappa\zeta) d\xi/\xi^2 \right\}$$

$$= \frac{\pi a^2 P}{1+\tau} + \pi a^2 P \int_1^{1+\tau} \psi(\xi,\zeta)\, \exp(-\kappa\zeta)\, d\xi/\xi^2 \qquad (A.3)$$

where

$$\psi(\xi,\zeta) \equiv (1+2\beta\xi^2)\mathrm{Cos}(\kappa\zeta\delta) + (1-2\xi-2\beta\xi^2)\tfrac{1}{\delta}\mathrm{Sin}(\kappa\zeta\delta) \qquad (A.4)$$

Up to any time $t>0$, the impulse delivered to the solid below plane $\mathcal{P}$, also normally directed, has amplitude $I(\tau)$ equal to $\int F(t')dt'$ over the time-interval $0 \le t' \le t$. That is, with $\zeta' \equiv \tau'-\xi+1$:

$$\frac{I(\tau)/P}{\pi a^2(a/c_p)} = \int_0^\tau \left\{ \frac{1}{1+\tau'} + \int_1^{1+\tau'} \frac{\psi(\xi,\zeta')}{\xi^2} \exp(-\kappa\zeta')\, d\xi \right\} d\tau' = \ln(1+\tau) + \int_0^\tau \int_1^{1+\tau'} \frac{\psi(\xi,\zeta')}{\xi^2} \exp(-\kappa\zeta')\, d\xi d\tau' \qquad (A.5)$$

In the (τ',ξ)-plane, the same triangular region is defined by $\{0 \le \tau' \le \tau;\ 1 \le \xi \le 1+\tau'\}$ as by $\{1 \le \xi \le 1+\tau;\ \xi-1 \le \tau' \le \tau\}$, or $\{1 \le \xi \le 1+\tau;\ 0 \le \zeta' \le \tau-\xi+1 \equiv \zeta\}$. It follows that

$$\frac{I(\tau)/P}{\pi a^2(a/c_p)} = \ln(1+\tau) + \int_1^{1+\tau} \int_{\xi-1}^{\tau} \frac{\psi(\xi,\zeta')}{\xi^2} \exp(-\kappa\zeta')\, d\tau' d\xi$$

$$= \ln(1+\tau) + \int_1^{1+\tau} \frac{1}{\xi^2} \int_0^{\zeta} \psi(\xi,\zeta') \exp(-\kappa\zeta')\, d\zeta' d\xi \qquad (A.6)$$

This last integral with respect to ζ' is elementary; noting that $\delta^2=-1+2/\kappa$, the indefinite integrals of $\exp(-\kappa\zeta')\ \mathrm{Cos}(\kappa\zeta'\delta)$ and $\exp(-\kappa\zeta')\ \mathrm{Sin}(\kappa\zeta'\delta)$ equal the functions $-\frac{1}{2}\exp(-\kappa\zeta')[\mathrm{Cos}(\kappa\zeta'\delta)-\delta\ \mathrm{Sin}(\kappa\zeta'\delta)]$ and $-\frac{1}{2}\exp(-\kappa\zeta')[\delta\ \mathrm{Cos}(\kappa\zeta'\delta)+\mathrm{Sin}(\kappa\zeta'\delta)]$, respectively. Hence:

$$\frac{I(\tau)/P}{\pi a^2(a/c_p)} = \ln(1+\tau) + \int_1^{1+\tau} \frac{d\xi}{2\xi^2} \left\{ \begin{array}{c} (1+2\beta\xi^2)+(1-2\xi-2\beta\xi^2) \\ -(1+2\beta\xi^2)\exp(-\kappa\zeta)[\mathrm{Cos}(\kappa\zeta\delta)-\delta\ \mathrm{Sin}(\kappa\zeta\delta)] \\ -(1-2\xi-2\beta\xi^2)\exp(-\kappa\zeta)[\delta\ \mathrm{Cos}(\kappa\zeta\delta)+\mathrm{Sin}(\kappa\zeta\delta)] \end{array} \right\}$$

$$= \frac{\tau}{(1+\tau)} - \int_1^{1+\tau} \frac{d\xi}{2\xi^2} \left\{ \begin{array}{c} (1+2\beta\xi^2)[\mathrm{Cos}(\kappa\zeta\delta)-\delta\ \mathrm{Sin}(\kappa\zeta\delta)] \\ +(1-2\xi-2\beta\xi^2)[\delta\ \mathrm{Cos}(\kappa\zeta\delta)+\mathrm{Sin}(\kappa\zeta\delta)] \end{array} \right\} \exp(-\kappa\zeta)$$

$$= \frac{\tau}{(1+\tau)} - \int_0^{\tau} d\zeta \left\{ \begin{array}{c} \beta[(1-\delta)\ \mathrm{Cos}(\kappa\zeta\delta) - (1+\delta)\ \mathrm{Sin}(\kappa\zeta\delta)] \\ -[\delta\ \mathrm{Cos}(\kappa\zeta\delta)+\mathrm{Sin}(\kappa\zeta\delta)]/\xi + \frac{1}{2}[(1+\delta)\ \mathrm{Cos}(\kappa\zeta\delta)+(1-\delta)\ \mathrm{Sin}(\kappa\zeta\delta)]/\xi^2 \end{array} \right\} \exp(-\kappa\zeta)$$

$$= \frac{\tau}{(1+\tau)} + \tfrac{1}{2}\,\beta\{(1-\delta)[\mathrm{Cos}(\kappa\zeta\delta) - \delta\ \mathrm{Sin}(\kappa\zeta\delta)] - (1+\delta)[\delta\ \mathrm{Cos}(\kappa\zeta\delta) + \mathrm{Sin}(\kappa\zeta\delta)]\}\ \exp(-\kappa\zeta)\,|_{\zeta=0}^{\tau}$$

$$+ \int_0^{\tau} d\zeta\ \{[\delta\ \mathrm{Cos}(\kappa\zeta\delta) + \mathrm{Sin}(\kappa\zeta\delta)]/\xi - \tfrac{1}{2}[(1+\delta)\ \mathrm{Cos}(\kappa\zeta\delta) + (1-\delta)\ \mathrm{Sin}(\kappa\zeta\delta)]/\xi^2\}\ \exp(-\kappa\zeta)$$

$$= \frac{\tau}{(1+\tau)} + \tfrac{1}{2}\,\beta\ [(1-2\delta-\delta^2)\ \mathrm{Cos}(\kappa\zeta\delta) - (1-2\delta+\delta^2)\ \mathrm{Sin}(\kappa\zeta\delta)]\ \exp(-\kappa\zeta)\,|_{\zeta=0}^{\tau}$$

$$- \tfrac{1}{2}\ [(1+\delta)\ \mathrm{Cos}(\kappa\zeta\delta) + (1-\delta)\ \mathrm{Sin}(\kappa\zeta\delta)][\ \exp(-\kappa\zeta)]/\xi\,|_{\zeta=0}^{\tau}$$

$$+ \int_0^{\tau} d\zeta\ \{[\delta + \tfrac{1}{2}\kappa(1+\delta)^2]\ \mathrm{Cos}(\kappa\zeta\delta) + [1 + \tfrac{1}{2}\kappa(1-\delta^2)]\ \mathrm{Sin}(\kappa\zeta\delta)\}[\exp(-\kappa\zeta)]/\xi \qquad \text{(A.7)}$$

As $\tau\to\infty$, the first line on the right side of Equation (A.7) becomes equal to $1+\frac{1}{2}\beta(\delta^2+2\delta-1)$. In the same limit, the second line vanishes ($\xi=1+\tau-\zeta$, so that $\xi=1+\tau$ when $\zeta=0$). The integral occupying the third line also vanishes then, as can be seen by dividing the interval of integration $(0,\tau)$ into (say) the two equal parts $(0,\frac{1}{2}\tau)$ and $(\frac{1}{2}\tau,\tau)$:

$$|\int_0^{\tau} d\zeta\ \{[\delta + \tfrac{1}{2}\kappa(1+\delta)^2]\ \mathrm{Cos}(\kappa\zeta\delta) + [1 + \tfrac{1}{2}\kappa(1-\delta^2)]\ \mathrm{Sin}(\kappa\zeta\delta)\}[\exp(-\kappa\zeta)]/\xi\,|$$

$$\le [2\delta+\kappa(1+\delta)^2]\int_0^{\tau}[\exp(-\kappa\zeta)]\ d\zeta/\xi = [2\delta+\kappa(1+\delta)^2]\left\{\int_0^{\tau/2}[\exp(-\kappa\zeta)]\ \frac{d\zeta}{\xi} + \int_{\tau/2}^{\tau}[\exp(-\kappa\zeta)]\ \frac{d\zeta}{\xi}\right\}$$

$$\le [2\delta+\kappa(1+\delta)^2]\left\{\int_0^{\tau/2}\frac{[\exp(-\kappa\zeta)]}{1+\tau/2}d\zeta + \int_{\tau/2}^{\tau}[\exp(-\kappa\zeta)]\ d\zeta\right\}$$

$$= [2\delta+\kappa(1+\delta)^2]\{\exp(-\kappa\tau/2) - \exp(-\kappa\tau) + [1-\exp(-\kappa\tau/2)]/(1+\tau/2)\}/\kappa \qquad \text{(A.8)}$$

The last line of Equation (A.8) vanishes as $\tau\to\infty$; so, therefore, must the integral on the first line (q.e.d.). It has thus been shown that [Equation (A.7)]:

$$I(\infty) = \pi[1 + \tfrac{1}{2}\beta(\delta^2+2\delta-1)](a^3/c_p)P \equiv \Lambda P \qquad \text{(A.9)}$$

Since Poisson's ratio ν fixes the constants β, κ and δ, Equation (A.9) dictates that if two systems have values of ν, a and c_p that make Λ the same for both, then the ratio of their cavity-wall pressures P_1 and P_2 will equal the ratio of the corresponding total impulses $I_1(\infty)$ and $I_2(\infty)$ delivered normal to plane $\mathcal{P}$ [$I(\infty)\underline{n}_{\mathcal{P}}$ is the total-impulse vector; $\underline{n}_{\mathcal{P}} \equiv$ unit normal to $\mathcal{P}$]. That is:

$$I_2(\infty)/I_1(\infty) = P_2/P_1 \qquad \text{(A.10)}$$

Systems with the same Λ-value [so that Equation (A.10) holds] include any two having the same value of both ν and a^3/c_p; those in turn include any two with the same values of ν, a and c_p, and *those* include any two with the same values of G, M, a and material density ρ.

On that same space-time domain (i.e., the domain of disturbance: $t \ge 0$, $0 \le r-a \le c_p t$), the radial displacement u_r is related to radial position and time as follows (ibid.):

$$u_r(\xi,\tau) \equiv u_r = \frac{aP}{2\kappa M\xi^2}\left\{1-[\mathrm{Cos}(\kappa\zeta\delta)+\tfrac{1}{\delta}(1-2\xi)\ \mathrm{Sin}(\kappa\zeta\delta)][\ \exp(-\kappa\zeta)]\right\} \tag{A.11}$$

Hence, if two systems have the same values of G, M and a, then the ratio of their displacements *at any given values of* ξ *and* τ will equal the ratio of their cavity-wall pressures; indeed, the ratio of their (u_r/a)-values will equal the pressure ratio if G and M alone are the same for both. Most important, if G, M, a and ρ are the same in the two systems, then [Equation (A.10)] the total-impulse ratio is also equal to the ratio of pressures, so that

$$[u_r(\xi,\tau)]_2/[u_r(\xi,\tau)]_1 = I_2(\infty)/I_1(\infty) \tag{A.12}$$

Note also that, with cavity radius (a) the same in both systems, a given value of ξ corresponds to the same radius r for both ($r=\xi a$); likewise, with M, a and ρ equal, a given value of τ corresponds to the same time in both ($t=a\tau\ /c_p$; $c_p^2=M/\rho$).

APPENDIX B

CONTAINED EXPLOSIONS IN SIMPLE MATERIALS: HOW CAVITIES FORM

Myriad conventional charges, and most nuclear ones, have been detonated in cavities of small radius (0-.4 $m/T^{1/3}$). Displacements of near-cavity material are then appreciable fractions of final cavity radii. The theory of explosions' effects on their surroundings, however, is better developed for bursts in so-called "big holes" (>2 $m/T^{1/3}$) than for small holes. Least well understood is the formation of craters by bursts shallow enough to produce them.

In brief, following explosive energy release in a big hole, the pressure of cavity gases can still be large enough to bring material around a cavity to its shear-strength limits. In such material, further outward displacement of the cavity wall then takes place without further increase in the difference between radial stress and hoop stress (at the wall, radial stress equals cavity pressure). Since containers (tires, for example) hold gas under pressure only by dint of differences between radial and hoop stresses in their walls, part of the pressure-load that would be opposed by hoop stresses in elastic wall material, is transferred to greater distances, where outward displacements increase as a result. At some medium-specific distance from the cavity, and beyond, stresses are too low to cause strength limits to be reached, and deformation is elastic. As a result, the whole system comes to mechanical equilibrium under (a) the residual pressure of cavity gases and (b) any stresses (e.g., overburden) present throughout undisturbed material. That happens sooner, and with less wall displacement, if the hole is so large that strength limits are not reached at all in adjacent material.

Patently basic to big-hole theory, and supported by its experimental validation, is the following idea: Geo-materials deform elastically during sufficiently small stress excursions about overburden, and they flow (i.e., move with shear stresses at limiting values) during larger excursions. For bursts in small holes, we therefore ask what results follow from assuming that flow at high stress, and elastic deformation at small stress, are the modes of behavior that dominate cavity growth. The relatively high pressures then felt by surrounding earth cause three important departures from the motion of material around a big hole: (i) An appreciable fraction of the explosive yield is converted to kinetic energy of the earth. (ii) Displacement of the cavity wall is large compared to its initial radius. (iii) Flow occurs out to ranges several times as large as the final cavity radius. Quasistatic and small-strain approximations suffice to describe displacements due to bursts in big holes, whereas, in view of (i) and (ii), the full equations of motion for arbitrary strains must be used to describe cavity growth from bursts in small holes. Item (iii) holds center stage here, however: Development of an extended region of flow profoundly influences not only the size of the final cavity, but its stability and the state of the surrounding medium, as will now be described.

B.1 SIMPLE MATERIALS.

Even when performed with elaborate material models, calculations of contained bursts in small holes almost always show that material near the cavity is left with permanent compressive stresses much larger than overburden. These stresses have their origin in basic properties of solids; as a result, their presence can be understood by considering simple materials. For present purposes, we therefore label as "simple" any isotropic material for which, in a spherical field: (A) Volume can change only elastically, (B) the difference between radial stress σ_r and hoop stress σ_θ cannot exceed a fixed limiting value Y (its "von Mises limit"), and (C) deformation is elastic as long as the resulting values of $|\sigma_r - \sigma_\theta|$ remain $<$ Y; otherwise the condition $|\sigma_r - \sigma_\theta| = Y$ holds during deformation, along with condition (A).

As background, note that in a spherically symmetric field: σ_r and σ_θ are principal stresses; shear stress varies with the orientation of the surface on which it is measured, and is zero on coordinate planes of any principal-axis system; the shear stress at a point is proportional to $\sigma_D \equiv \sigma_r - \sigma_\theta$, and its maximum value ($\frac{1}{2}|\sigma_D|$) acts on any plane that makes a 45° angle with the radial direction. From these facts, it follows that the constraint $|\sigma_D| \leq Y$ [condition (C)] does no more (nor less) than limit the ability of simple materials to support shear stress – in accord with a core property of real materials. Also, if the shear stress attains its limiting value $\frac{1}{2}Y$ in a simple material, it does so on planes at 45° to the radial. Most important: If the shear stress on such a plane (its maximum at any given point) is maintained at its limiting value in a simple material, then any slippage that occurs along the plane generates no opposing stresses. By contrast, at smaller maximum shear stresses than that limit, even a slight additional shearing along the plane will cause an opposed increase in shear stress.

B.2 RESIDUAL, OR "LOCKED-IN" STRESS.

Consider now the behavior of simple materials in uniaxial strain (which spherical deformation becomes in the limit of large radius). In particular, with σ_r and σ_θ denoting axial and lateral stress, respectively, let an element of simple material be subjected to uniaxial compression ($\sigma_r > 0$) and then unloaded back to $\sigma_r = 0$. Loading is at first elastic [condition (C)]; σ_θ will increase in the materials of greatest interest (e.g., linear elastic materials with positive Poisson's ratio, ν), but not as much as σ_r does [except in fluids, whose shear stress is always zero (at least quasistatically)]. Hence, σ_D ($=\sigma_r - \sigma_\theta$) increases with σ_r until its limiting value Y is reached. Further growth of the axial load σ_r results in added compression, but σ_D remains equal to Y. Thus, once σ_D reaches the value Y, increases in compression no longer give rise to increases in shear stress, but only to increases in mean stress $\bar{\sigma}$ [$\equiv \frac{1}{3}(\sigma_r + 2\sigma_\theta)$]. Yet, further axial compression is automatically attended by more shear deformation. In contrast with earlier loading (when $\sigma_D < Y$), however, that deformation no longer

generates opposing stresses. Hence, resistance to uniaxial compression drops when σ_D attains its limiting value Y; a compressive increment in σ_r causes a larger decrease in volume if the material flows ($|\sigma_D|$=Y) than if it deforms elastically ($|\sigma_D| < Y$).

Unloading, which is initiated when σ_r has reached a maximum value Σ_r, relieves shearing stresses (and others). As a result (since shear stress is proportional to σ_D), σ_D falls from its limiting value Y as unloading begins, and unloading proceeds elastically. As already noted, however, the material is less compressible elastically than when it flows, Hence, the element expands less when σ_r is reduced from Σ_r to zero, than it shrank on increasing σ_r from zero to Σ_r. The net effect of the load-unload cycle is therefore to leave the element with residual compression, and hence [condition (A)] with residual compressive mean stress. Moreover, since σ_r=0 after unloading, it follows that the final value of σ_θ is compressive. Thus, lateral compressive stress remains in the element as a result of its having flowed during compression. Hereafter, such residual stresses are termed "locked-in" stresses.

If Σ_r is large enough, then a complication to the load-unload cycle just described is met: $|\sigma_D|$ will reach its limiting value on unloading (σ_D=–Y). In particular, just as in elastic loading, σ_θ does not change as rapidly as σ_r on unloading, so that $|\sigma_D|$ would continually increase if either elastic loading or unloading were to continue indefinitely. Once the limiting shear stress –Y is reached in unloading, therefore, $\sigma_D=\sigma_r-\sigma_\theta$ must remain at the value –Y. Since σ_r=0 on complete unloading, it follows that the locked-in stress σ_θ cannot exceed Y. For materials whose elasticity is linear, the limiting locked-in stress Y is found whenever $\Sigma_r \geq \sigma_r^*$, where $\sigma_r^*=(c_L/c_S)^2Y$ and the material's longitudinal and shear-wave speeds, respectively, are c_L and c_S [$(c_L/c_S)^2$=M/G]. In fact, flow then starts when $\sigma_r=\frac{1}{2}\sigma_r^*$, and the locked-in stress increases linearly with Σ_r from zero to Y for values of Σ_r from $\frac{1}{2}\sigma_r^*$ to σ_r^*. For a simple material whose elasticity is linear, Figure B-1 illustrates the stages of a load-unload cycle of uniaxial strain.

As for spherical fields, hoop strains play a major role in their development (B.3 below). As a result, stress paths depart somewhat from those of uniaxial strain during compressive loading, and on subsequent unloading the differences are large (B.4). Still, when a simple material is driven by a shock or a steeply rising compression pulse to states in which $\bar{\sigma} >> Y$, a locked-in hoop stress about equal to Y can be expected after unloading. Accordingly, to the extent that elasticity and flow exhaust the modes of deformation of material near an actual explosively formed cavity, that material should afterward contain locked-in stresses of a size comparable to its strength. For such events, computational models of geo-materials are not "simple," but elasticity and flow do dominate their calculated behavior near the cavity – and the models do yield radial distributions of locked-in stress of the expected size. We now recall how those distributions evolve.

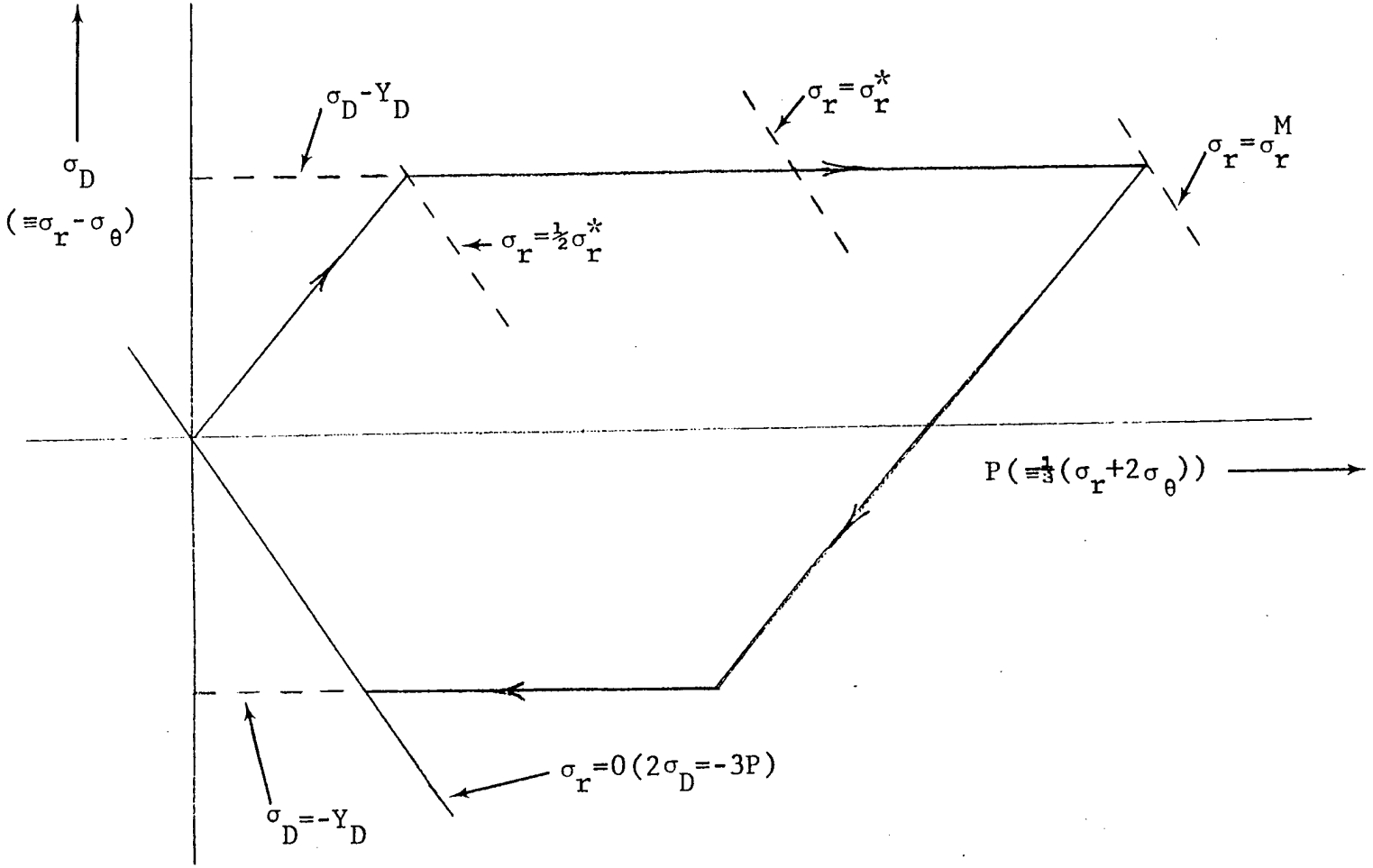

Figure B-1. Schematic of stress-path followed when a simple linear material (Poisson's Ratio = $\frac{1}{4}$) is loaded and unloaded in uniaxial strain, starting at zero stress. Deformation is elastic until the axial load σ_r reaches $\frac{1}{2}\,\sigma_r^* = \frac{1}{2}\sqrt{c_L/c_S}\;Y_D$, where c_L and c_S are longitudinal- and shear-wave speeds, respectively, and Y_D is the maximum possible value of $|\sigma_D|$. Unloading begins when $\sigma_r = \sigma_r^M > \frac{1}{2}\sigma_r^*$. If $\sigma_r^M < \sigma_r^*$, unloading is complete before σ_D attains the limiting value $-Y_D$; otherwise σ_D has the final value $-Y_D$. For any initially-hydrostatic stress state, the load-unload diagram is congruent to that shown.

B.3 THE "ATLAS ZONE" AND ITS DEVELOPMENT.

As calculated using diverse material models (many quite complex) and discretized equations of motion (but otherwise exact), cavity growth ends for contained bursts at about $2\frac{1}{2}$ (but less than 4) $ms/T^{1/3}$. The final cavity radius greatly exceeds the value it would attain by quasistatic expansion (B.5, below) and the final cavity pressure is often smaller than overburden. Hence, the cavity is not held open by the pressure of gases within. Instead, the forces that hold it open in stable equilibrium with the surrounding earth are supplied by locked-in stresses. Those stresses develop during cavity growth over the region of inelastic deformation, which covers a spherical shell of finite thickness bounded by the cavity wall. Since its stresses support the load of an adjoining world, that shell (more precisely, an inner core thereof; B.5) is referred to here as the "Atlas Zone." To see how an Atlas Zone forms, consider a tamped, spherically symmetric explosion in homogeneous simple material, under a uniform overburden great enough to preclude cracking. Development of an Atlas Zone then takes place as follows.

Pressures of 10-to-20 GPa from conventional explosives (a hundred times that in nuclear bursts) drive nearby material away from the burst point at high speed, as cavity growth begins. As a result, when the pressure in the cavity falls to overburden levels, material near the wall is still moving outward. Further deceleration of wall material then occurs, as before, because cavity pressure continues to drop, and because radial stresses are more compressive than hoop stresses [which makes for negative acceleration; Equation (2.1)].

The stress difference σ_D ($\equiv \sigma_r - \sigma_\theta$) remains at its von Mises limit Y through almost the entire time of cavity growth, despite the drop in cavity pressure, owing to continually increasing hoop strains. That is, expansion of the cavity causes rings of material around it to stretch, constantly driving hoop stresses toward tensile values, whereas radial stresses at the cavity wall must equal the (compressive) cavity pressure. The difference σ_D between radial and hoop stresses is then constant at Y>0, and hence acts [Equation (2.1)] as a source of inward acceleration – a constant deceleration as material slows (ignoring small fractional changes in its radius). Once *velocity* becomes inward-directed, however, hoop strains and stresses grow more compressive and σ_D decreases from Y: As inward motion proceeds, material deforms elastically near the cavity wall.

Now, in states of shear failure, unlimited deformation can occur with no change in stress (B.1), but elastic deformation is always attended by opposing stress-changes. Inward motion therefore gives rise to ever-growing stresses to oppose that motion (in salt, for example, an elastic decrease in cavity radius by 1% would produce a compressive hoop-stress increase of a few tenths of a GPa). As a result, when

the straining that causes inward acceleration of wall material finally arrests its outward motion, no more than a slight decrease in cavity radius can occur without generating compressive hoop stresses that would impart large outward acceleration to the wall. In the event, the wall's velocity falls continuously to zero and then turns negative. The resulting compressive hoop-stress increments – locked-in stresses of the kind discussed above (B.2) – therefore simply arrest its inward motion before any large inward velocity develops: After reaching its maximum radius, the wall oscillates with negligible (and decreasing) amplitude about its final equilibrium position.

B.4 LOCKED-IN STRESS: THE SALMON EVENT.

As already noted (B.2, above), the stress paths traced in spherical bursts differ substantially from the paths (Figure B-1) followed in uniaxial strain. In particular, for reasons stated in Section B.3, the wall and nearby earth continue to *flow* as they slow down. Hence, as pressure falls in the expanding cavity, unloading occurs largely along the limiting stress path $\sigma_D \equiv \sigma_r - \sigma_\theta = Y$: Loading stress-paths (which do resemble that of Figure B-1 for uniaxial strain) are in large part retraced on unloading (strain paths are not). With the onset of *inward wall motion* (negative radial velocity), further unloading takes place elastically and with almost constant pressure at the cavity wall (B.3). Stress paths for elastic unloading at constant $\sigma_r > 0$ are therefore parallel to the line $\sigma_r = 0$ in Figure B-1 – and final states are reached by material near the wall along paths parallel to that one.

Since the wall reverses direction sooner than material further out, an elastic unloading wave spreads outward through the region of flowing material. The development of large compressive hoop stresses requires little inward motion, however (B.3), and stops such motion after only slight inward displacement. Radial stresses are larger in the interior of the flow region than at the wall (B.5; also, falling gas pressure is felt first at the wall), and hence are not fully relieved by that displacement. Thus, as motion winds down near the cavity, a characteristic stress-pattern emerges, of which an example is discussed in the rest of this section: Hoop stress has its maximum compressive value at or very near the cavity wall, and then decays smoothly with radius through the flow region. Radial stress, which is equal at the wall to the final gas pressure, rises to a maximum at a somewhat larger radius; spherical divergence (presumably) causes stress-decay at still larger radii (geometric attenuation of displacement, stress, etc., with radius is especially rapid on the region of flow, which abuts the cavity and contains all locked-in stress).

The processes just described, and also those of Section B.3, are evident in stress and radial-velocity wavetrains (Figures B-2 and B-3, respectively) from an ATI calculation of the Salmon event. As modeled therein, the strength of dome-salt increases smoothly with mean stress $\overline{\sigma}$ (from 4 MPa at $\overline{\sigma} = 0$

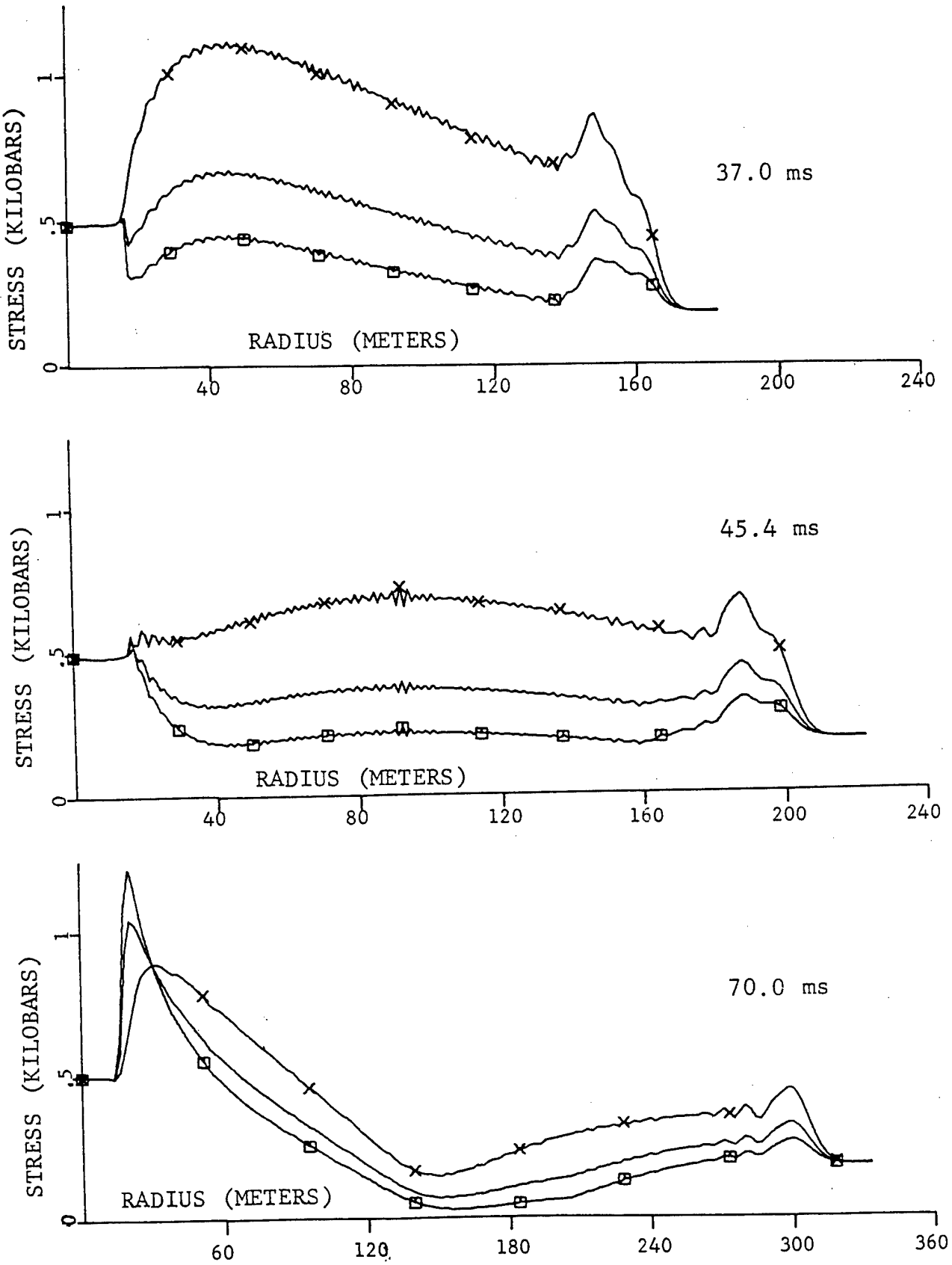

Figure B-2. Stress vs. slant range, calculated for the Salmon Event 37.0, 45.4 and 70.0 milliseconds (ms) after the burst. Radial and hoop stresses are shown, respectively, by curves marked "×" and "□"; unmarked curves refer to mean stress.

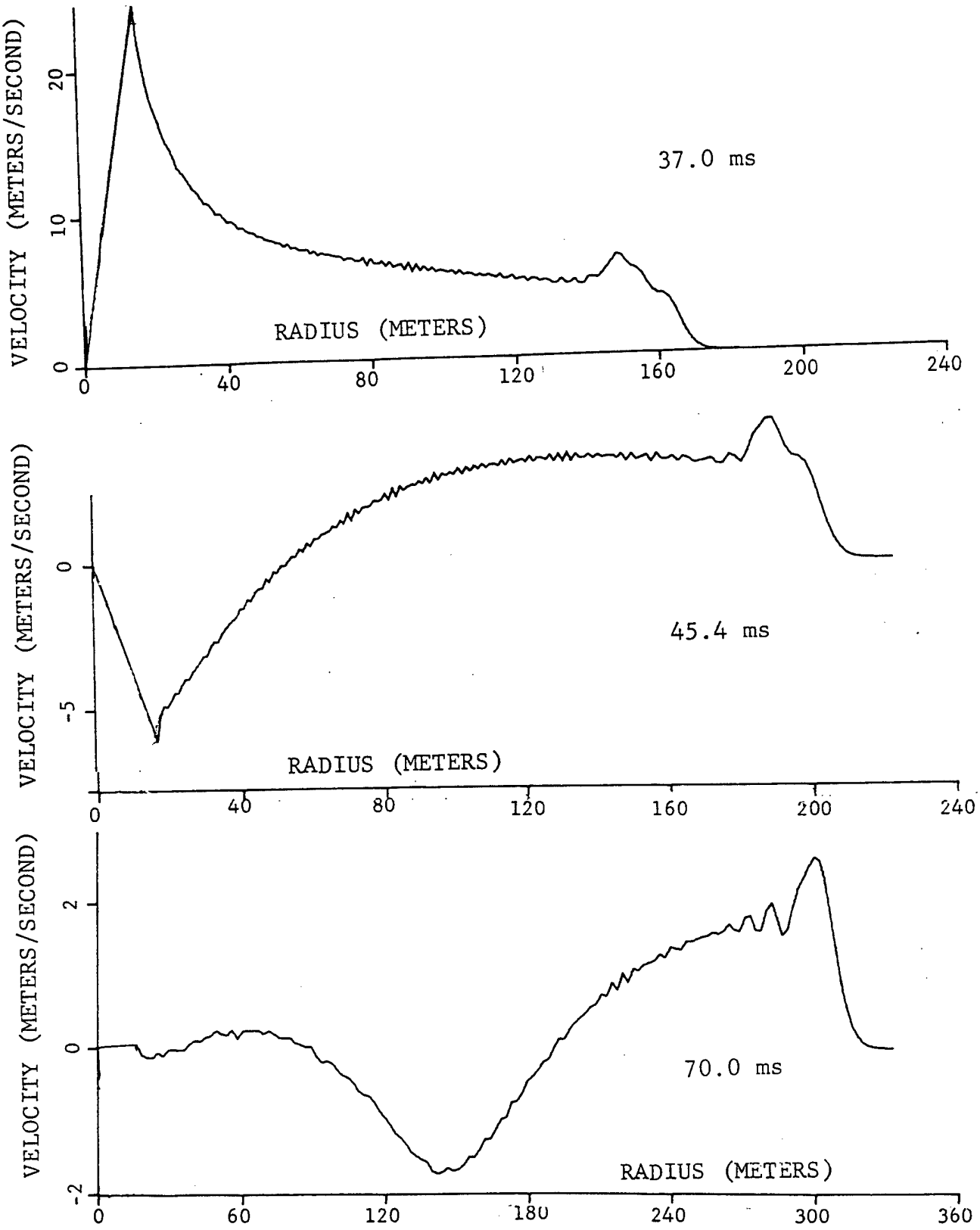

Figure B-3. Radial particle velocity vs. slant range, calculated for the Salmon Event 37.0, 45.4 and 70.0 milliseconds (ms) after the burst.

to 41 MPa at $\bar{\sigma}$=50 MPa, to 87 MPa for $\bar{\sigma} \geq 220$ MPa); the model also admits inelastic changes in volume. In the calculation, the cavity wall moves outward for ~ 42 ms after its motion starts. At 37 ms, the medium is flowing at all points between the wall ($R_c \approx 16$ m and moving outward at ~ 25 m/s; Figure B-3) and a local peak almost nine cavity radii further out (near the wavefront; Figure B-2). By 45.4 ms, the wall is moving inward (at ~ 7 m/s), and material is unloading elastically from R_c (the wall-radius) out to $\sim 2R_c$. At 70 ms, near-static equilibrium has been reached from R_c (still ≈ 16 m) to $6\frac{1}{4}R_c$. Evidence of that lies in small-to-negligible radial velocities over the region noted. More compelling: At static equilibrium, σ_r must equal σ_θ wherever $\partial\sigma_r/\partial r=0$ [Equation (2.1)], and, in Figure B-2 at 70 ms, hoop stress does equal radial stress at a point very close to the latter's maximum (defined here as the outer radius of the Atlas zone; Section B.3). Thus, the figure's peak hoop stress ($\sim .100$ GPa above an overburden of 18 MPa) is locked into the medium.

For particles of salt that end up at $\frac{3}{2}R_c$, $4R_c$ and $8R_c$, Figure B-4 presents the stress paths traced in reaching final states of stress. Evidently, after a brief elastic stage, loading takes place at the limit of shear stress ($\sigma_D \equiv \sigma_r - \sigma_\theta$=Y), which, on this model, is reduced by shock heating (such reduction, a slight one, can be seen on path $\frac{3}{2}R_c$, but not for more distant material). Further, until the final stress-state is approached, most *un*loading also takes place mainly at that limit; path $4R_c$ departs from it somewhat (as do other paths) when, for a short time after the initial rise to peak compression (loading), σ_r decreases faster than σ_θ. Soon after material starts moving inward, however, its unloading proceeds elastically. Near the cavity wall, where σ_r is about equal to cavity pressure P, that happens at once: With P (hence σ_r) much less sensitive than hoop stress σ_θ to elastic decreases in wall-radius, σ_D falls from its shear-failure value Y if elasticity is *assumed* [even though inward motion of the wall makes both σ_θ and P (hence σ_r) less tensile] – whence changes in strain must *be* elastic. Elastic behavior ensures a large drop in σ_D without much inward displacement – hence little change in P – and, perforce, in σ_r. Elastic unloading (its final stage) therefore unfolds near the cavity-wall in the general direction of lines of constant σ_r (Figure B-1), as Figure B-3 affirms.

B.5 CAVITY SIZE AND ELASTIC TRANSPORT: DYNAMIC AND GEOMETRIC EFFECTS.

The fact that large strains develop near contained spherical bursts in small holes (0-.5 $m/T^{1/3}$ radius), follows from the cavities' large ratios of final radius to initial radius. By the same token, strains are large even around quasistatically pressurized cavities (to burst-like pressures). Hence, cavity growth is inherently nonlinear, as shown by the quasistatic elasto-plastic result that final cavity radius grows exponentially with cavity pressure (above the least pressure at which the wall fails in shear; Hill, loc. cit.). Quasistatic release of explosive energy in a small cavity results in a final radius of $\sim 1.19\ Y^{-2/9}$ $m/T^{1/3}$, where Y, in MPa, is the maximum of $Y(\bar{\sigma})$ [e.g., 87 MPa for the salt model of Section B.4;

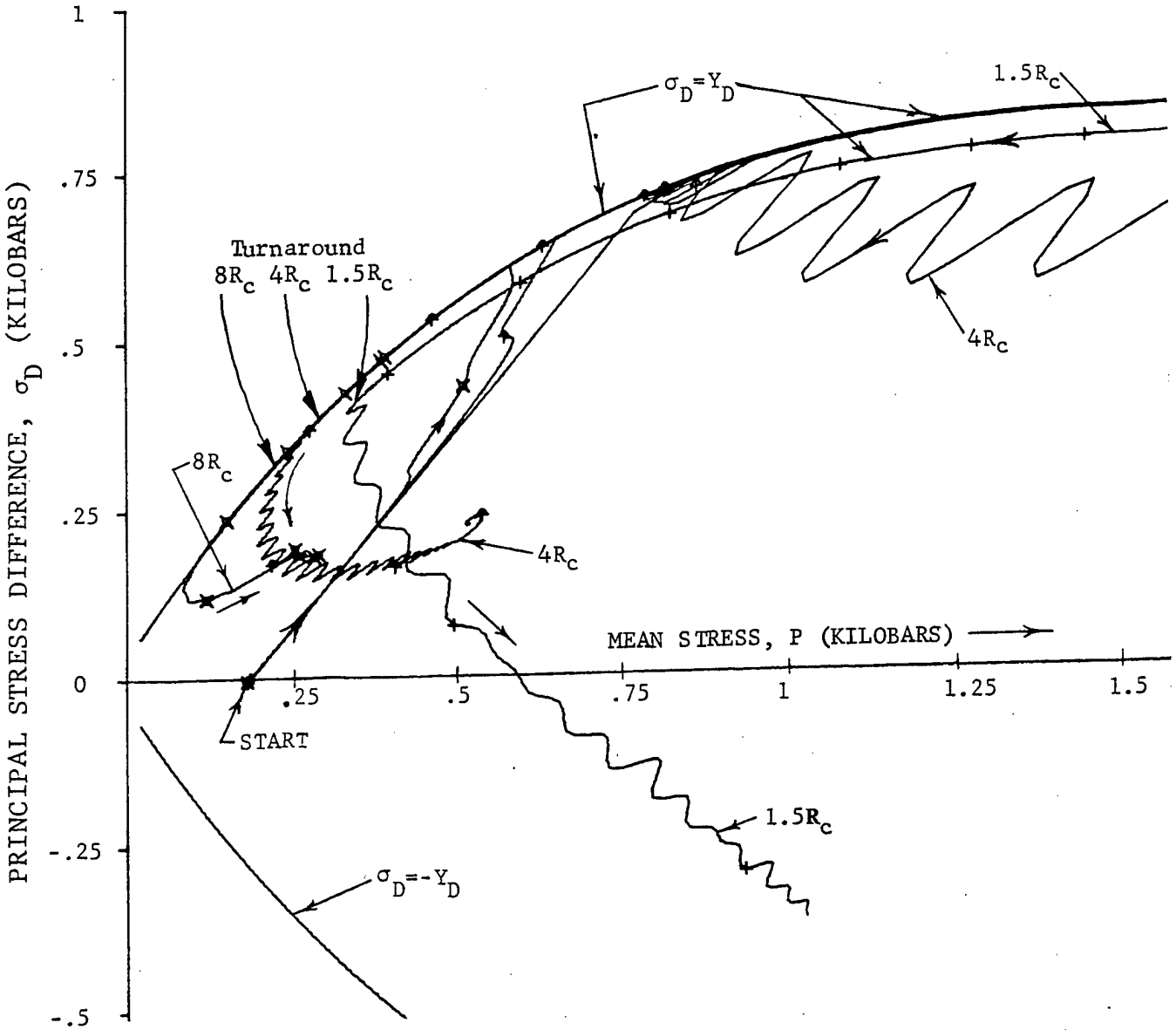

Figure B-4. Calculation of the Salmon Event: Stress-paths followed by sample particles at final radii equal to 1.5, 4 and 8 times the cavity radius, R_c. In all cases, compressive loading starts from a hydrostatic state at .181 kb of mean-stress (the overburden), and quickly takes the shear-stress (and hence the stress difference σ_D) to limiting values, where they remain until loading ends. At 1.5 R_c and 4 R_c, peak values of mean stress are to large to be shown on the plot. Most subsequent unloading takes place with σ_D retracing the same limiting values traversed on loading. In its final stage, unloading is elastic, and radial stresses increase at 1.5 R_c and 8 R_c. In the computational salt medium, shear strength (and hence limiting values of σ_D) vary with internal energy as well as mean stress; thermal effects on strength are insignificant at 4 R_c and 8 R_c, but noticeable at 1.5 R_c. Also, inelastic volume increases ("bulking"), attend shear failure, while inelastic decreases in volume ("compaction") take place in hydrostatic compression.

writing $Y(\bar{\sigma})$ distinguishes strength-as-a-function-of-mean-stress-$\bar{\sigma}$ from its maximum value Y]. Dynamic effects (due to explosive release of energy) increase the final radius to $\sim 2.86\ Y^{-2/7}\ m/T^{1/3}$.

The first of these two expressions fits closely an accurate pencil-and-paper solution to the quasistatic problem. The second is a close fit to results obtained by massive computing (using discretized equations of motion) for spherical bursts in simple materials. So far, it has nonetheless proven accurate to within $\pm 25\%$ for media with porosities $< 5\%$ and $Y \leq 170$ MPa, with above-average radii obtained (usually) in the fields computed for non-simple materials. More important, final cavity radii measured for contained tamped explosions are also larger – about $1.0\ m/T^{1/3}$ for ordinary and nuclear explosives (the formula gives $.80\ m/T^{1/3}$ for dome-salt). At that radius, accepted equations of state for cavity gases (vaporized earth, in essence, for nuclear bursts) yield pressures of $\sim .28$ GPa if all energy stays in the cavity; massive computing leaves $\frac{1}{5}$ to $\frac{3}{5}$ of the energy in the cavity when it stabilizes, which implies that final cavity pressures are generally < 100 MPa (chemical explosive) and 50 MPa (nuclear).

Seconds, it should be noted, are long compared to the times called "final" here (Section B.4); over much longer times still, cavity gases cool (or may diffuse into nearby soil/rock) and their pressures drop by large factors. Salmon presents a dramatic case in point: Re-entry drilling disclosed a cavity whose pressure, six months after the event, had fallen to .03 MPa – a partial vacuum inside a cavity of 16.7-m radius ($.96\ m/T^{1/3}$; Rawson, et al., 1966). Moreover, at times of a second or less, an appreciably larger radius (by a factor of almost 1.5) has been postulated for the Salmon cavity (reduced by creep to 16.7 m over six months' time; Rogers, 1966). As estimates of actual "final" pressures, values up to 100 MPa (chemical) and 50 MPa (nuclear) could therefore be excessive. On the other hand, σ_r attains values much greater than σ_r^* near the wall (Section B.3), because wall-pressure does – and, in media well described as simple, locked-in stresses therefore reach the maximum value possible in the initial shock (i.e., in uniaxial strain). That value, Y, most likely exceeds the "final" cavity pressure. Whether it does or not, however, *geometry* magnifies the part played by locked-in stress (relative to gas pressure) in holding open a final spherical cavity – as we now explain.

The instructive geometric object (Figure B-5) is part of a right circular cone of small angle θ with its vertex at the burst point – a frustum, in the limit $\theta \to 0$. For finite θ, the cone-segment $\mathcal{F}$ in question runs from the (spherical) cavity-wall at its "final" radius R_C to the spherical sheet of material whose radius R_F at "final" equilibrium bounds the region of flow. That is, end-caps – sections of spherical surfaces centered at the cone's vertex – truncate the cone to form $\mathcal{F}$; further, material at $\mathcal{F}$'s outer end-cap has undergone shear failure and $\mathcal{F}$ holds all cone material that ever has so failed. Symmetry makes the normal to $\mathcal{F}$'s surface at any point a principal-stress (and -strain) axis, so that traction thereon is normally directed. In the direction of the cone's axis, which is radial, the force *on* an areal element of

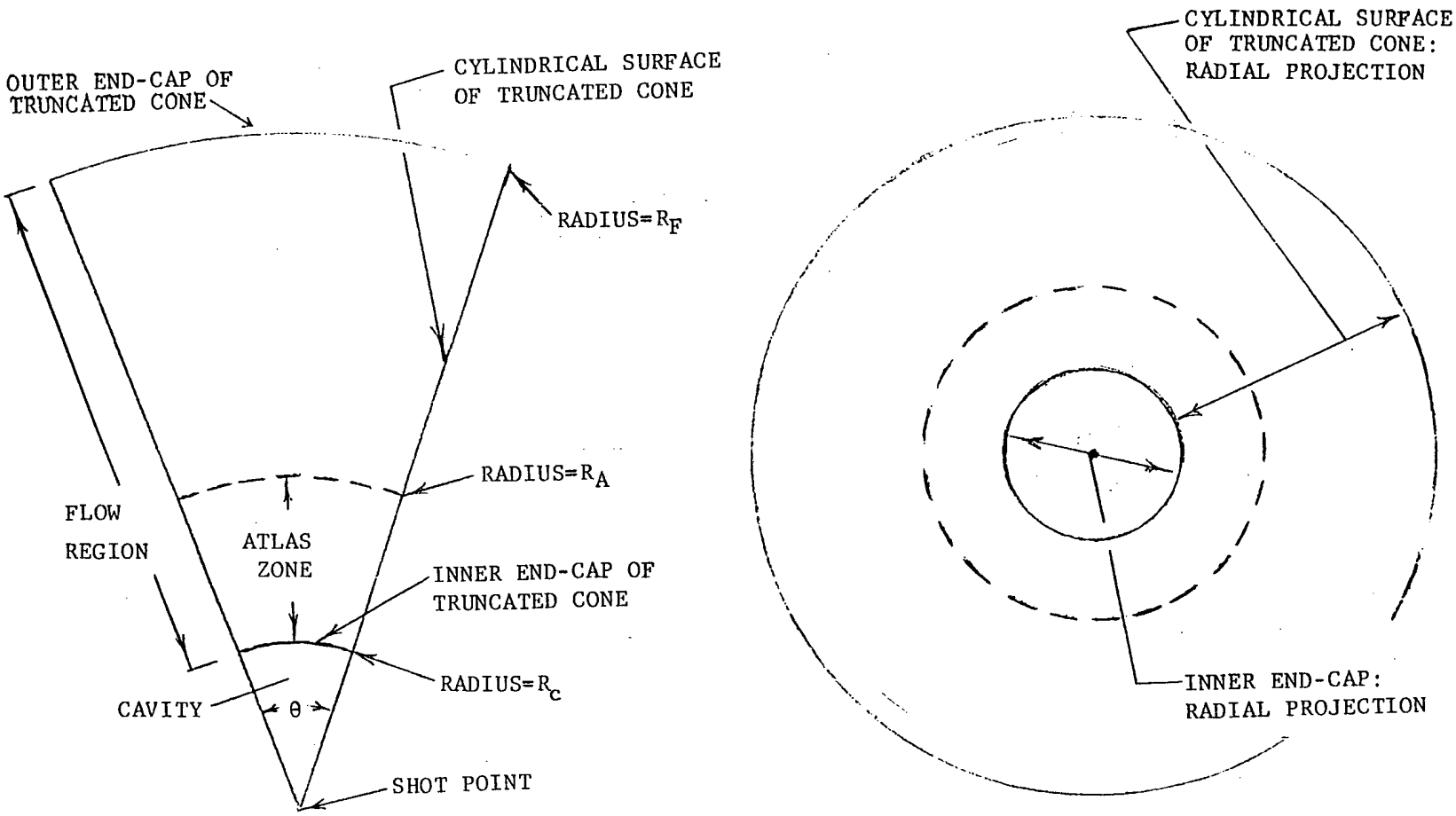

Figure B-5. Schematic of conical region extending outward from the shot point, showing the cavity, region of flow and Atlas zone created by an explosion in a small hole.

$\mathcal{V}$'s surface is thus equal to the element's area, times the normal traction there (hoop stress over the conical surface, radial stress on the end-caps), times the axial (i.e., radial) component of the *inner* normal to the element. In turn, the product of the normal's axial component with the element's area is just the area of the element's projection on any plane normal to the cone's axis.

The projection of the inner end-cap on such a plane is clearly a circle of radius $R_C \mathrm{Sin}\frac{\theta}{2}$ [and area $\pi R_C^2(\mathrm{Sin}\frac{\theta}{2})^2$]; since, over the whole cap, normal traction equals final wall pressure $P^{\check{}}$, the radial force F_C on that cap is $P^{\check{}}\pi R_C^2(\mathrm{Sin}\frac{\theta}{2})^2$. In the same plane, the projection of $\mathcal{V}$'s conical surface is evidently an annulus of inner radius $R_C \mathrm{Sin}\frac{\theta}{2}$ and outer radius $R_F \mathrm{Sin}\frac{\theta}{2}$, but hoop stress (normal traction) thereon varies with radius; accordingly, the radial force F_L delivered to the conical surface is the product of its projected area $\pi(R_F^2-R_C^2)(\mathrm{Sin}\frac{\theta}{2})^2$ with an average ($\bar{\sigma}_{\theta}^{\check{}}$, say) of the values of final hoop stress $\sigma_{\theta}^{\check{}}$ over said surface. Thus, as the ratio $(\sigma_{\theta}^{\check{}}/\ P^{\check{}})(R_F^2-R_C^2)/R_C^2$ of the two radial forces shows, the geometric factor $(R_F^2-R_C^2)\ /R_C^2$ magnifies the contribution of locked-in hoop stress to the outward force on the cone, relative to that of cavity pressure; the factor is 3 if R_F is just twice R_C, but it can be much greater [for Salmon (Figure B-3, bottom) $\sigma_{\theta}^{\check{}}$ actually *exceeds* $P^{\check{}}$ out to $\sim 3R_C$, and $R_F \approx 10\ R_C$] .

The force F_E (radially inward) exerted *on* the outer end-cap is equal to $-\sigma_E^{\check{}}\pi R_F^2(\mathrm{Sin}\frac{\theta}{2})^2$, where $\sigma_E^{\check{}}$ denotes the final radial stress at R_F (the elastic-plastic radius); F_L, expressed exactly in terms of $\sigma_{\theta}^{\check{}}$, equals $\int\sigma_{\theta}^{\check{}}\pi\ \mathrm{d}(r\mathrm{Sin}\frac{\theta}{2})^2=\pi(\mathrm{Sin}\frac{\theta}{2})^2\int\sigma_{\theta}^{\check{}}\mathrm{d}r^2$, over $R_C \le r \le R_F$. Since $F_C+F_L+F_E$ must equal zero at equilibrium, the force $-F_E$ $[=\sigma_E^{\check{}}\pi R_F^2(\mathrm{Sin}\frac{\theta}{2})^2]$ delivered to unfailed cone-material across the elastic-plastic boundary ($\mathcal{V}$'s outer end-cap, at radius R_F) must equal F_C+F_L. Given purely elastic deformation beyond R_F, final radial displacement there is determined by $\sigma_E^{\check{}}$ (plus the overburden at huge radii where, physically, the burst cannot effect finite changes) – and, $\sigma_E^{\check{}}=(F_C+F_L)/R_F^2$. Indeed, the displacement at any $r \ge R_F$ is *proportional* to $\sigma_E^{\check{}}$ if the state of zero stress is defined as that of the pre-shot medium (whereupon overburden is zero by definition); $\sigma_r^{\check{}}$ (for example) is then automatically the permanent *change* in radial stress, at a given field-point, wrought by the burst [initial stresses are otherwise subtracted from $\sigma_{\theta}^{\check{}}$, etc., in the formulas above – which still remain valid because, over a closed surface in any equilibrium field (including the initial field), the net force is zero].

The spherical sheet of material that ends up at R_F could, mathematically at least, have started out at a radius $\ge R_F$. Given purely elastic deformation outside that sheet, however, the change in radial stress at R_F would then be zero or tensile, even though the volume of solid between the cavity and R_F has decreased and all volume changes are elastic. On its face, such an outcome flouts physical sense, which lies instead (for example) with an exact *quasistatic* result for simple materials: At the elastic-plastic boundary, the change in radial stress ($\frac{2}{3}$Y; Hill, loc. cit.) is compressive. As for Salmon, near-equilibrium obtains at the last time shown (Figure B-3) only out to $r \approx 6R_C$, whereas $R_F \approx 10\ R_C$.

Still, to $6R_C$, we find $\check{\sigma_\theta}>0$ (i.e., hoop-stress changes are compressive), and the same holds for radial stress (Figure B-2); results of the calculation at later times (not shown) have $\check{\sigma_\theta}>0$ out to R_F. Thus, not only is $F_L>0$ (indeed, $\int\check{\sigma_\theta}dr^2$ increases steadily with r), but geometry renders F_C (also >0) << F_L. The change $\check{\sigma_E}$ in radial stress at R_F must again be compressive (since $F_C+F_L>0$), so that material comes to rest there after a net outward displacement; the computed field directly confirms these things.

The great resistance of simple media to elastic changes in hoop strain provides general reason to expect such results. True, inward motion at and near the cavity wall is opposed by increasing pressure thereon; the modulus $3\gamma P$ (3P to 4P) relates increments in wall-pressure P (hence radial stress) and hoop-strain [Cooper, 1966, Equation 6]. By contrast, with σ_r=P, the modulus relating increments in hoop-stress and -strain is $3\gamma P\lambda/M+\varepsilon M$, where ε is ≥ 1 for $0 \leq \nu \leq \frac{1}{3}$ [$\varepsilon \equiv (1-2\nu)(1+\nu)/(1-\nu)^2$]. With P<.1 GPa, M far exceeds $3\gamma P$ [Salmon: $M/(3\gamma P)>100$]. Hence, inward motion (elastic unloading) near the wall is resisted mainly by hoop-stress growth; locked-in hoop stress, not gas pressure, keeps the cavity open. Further, as inward motion is arrested and equilibrium impends, that sharp growth (relative to radial stress) takes hoop stress to compressive levels above those of radial stress (up to the limiting stress-difference Y). At the same time, spherical convergence during inward motion drives up mean-stress values, which tends to increase radial stress near the cavity – except at the wall, where σ_r must equal P. The outlines of an equilibrium stress-distribution on the flow region thus emerge: Hoop stress rises to a peak, and exceeds radial stress, very near the wall; radial stress increases more gradually with radius, but must eventually exhibit the decay that spherical divergence demands – and, at its peak, σ_r must equal σ_θ (Section B.4).

At the opposite extreme (big holes, full decoupling), no flow takes place at all (R_F=R_C). Particle displacements, including that of the cavity wall, then result solely from a permanent change in cavity pressure. In all cases, though, F_C (gas pressure) and F_L (locked-in stress) determine radial stress, and hence displacement, at the elastic-plastic boundary (r=R_F). In turn, that displacement determines how much of the cavity's volume is transported elastically to distant parts – just as mean stress locked into the flow-region fixes the volume added to the cavity by elastic compression of solid on that region. The ratio $F_L/(F_C+F_L)$ measures the importance of locked-in stress to the final field of displacement. Its value is ≈ 1 for tamped bursts [>1 if $\check{P}<0$ (final gas pressure < overburden) – no miracle], and decreases to zero as hole-size increases to the minimum level for full decoupling.

In sum: Residual gas pressure dictates the displacement field left by an explosion in a large hole. For bursts in small holes, residual (locked-in) stress in the host medium determines permanent displacement. Calculations set the radii of "small" holes at 0-to-$\frac{1}{2}$ $m/T^{1/3}$; holes with radii >2 $m/T^{1/3}$ are "large." These results hold if inelastic volume decreases on the region of flow aggregate to a small

fraction of final cavity volume, and if deformation is elastic outside the region of flow. That is, they hold for the geologic media envisioned by big-hole theory.

DISTRIBUTION LIST

DSWA TR-95-95

DEPARTMENT OF DEFENSE

DEFENSE INTELLIGENCE AGENCY
ATTN: TWJ

DEFENSE SPECIAL WEAPONS AGENCY
ATTN: ESA, MAJ SNOW
2 CY ATTN: OSIA
2 CY ATTN: TRC
ATTN: WEL
ATTN: WEL, L WITTWER
ATTN: WEP, W ULLRICH

DEFENSE TECHNICAL INFORMATION CENTER
ATTN: DTIC/OCP

FC DEFENSE SPECIAL WEAPONS AGENCY
ATTN: NVCG

FC DEFENSE SPECIAL WEAPONS AGENCY
ATTN: FCT-Q, E RINEHART
ATTN: FCTO
ATTN: FCTT, DR BALADI
ATTN: FCTTS, R HENNY
ATTN: FCTTS, E TREMBA

DEPARTMENT OF THE ARMY

DEFENSE ADVANCED RESEARCH PROJECTS AGENCY
ATTN: RMO RETRIEVAL

U S ARMY ENGR WATERWAYS EXPER STATION
ATTN: CEWES-SD-R, J ZELASKO

DEPARTMENT OF THE NAVY

NAVAL SURFACE WARFARE CENTER
ATTN: CODE K42, R ROBINSON
ATTN: CODE K42, S HUGHES

DEPARTMENT OF THE AIR FORCE

AF TECHNICAL APPLICATIONS CENTER
ATTN: ROBERT BLANDFORD

AFSOR/NP
ATTN: COL JERRY PERRIZO

AIR FORCE TECHNICAL APPLICATIONS CTR
ATTN: FRANK PILOTTE, TT
ATTN: GEORGE ROTHE, TTR

GEOPHYSICAL LABORATORY
ATTN: JAMES LEWKOWICZ
ATTN: XO

DEPARTMENT OF ENERGY

LAWRENCE LIVERMORE NATIONAL LAB
ATTN: L - 15, TODD HOOVER
ATTN: L - 200, D B CLARKE
ATTN: L - 205, WILLARD J HANNON, JR
ATTN: L - 84, G POMYKAL

LOS ALAMOS NATIONAL LABORATORY
ATTN: D218, MS M HENDERSON
ATTN: ESS - 4, PAUL JOHNSON
ATTN: R KIRBY
ATTN: TECH LIBRARY

SANDIA NATIONAL LABORATORIES
ATTN: J M MCGLAUN
ATTN: T K BERGSTRESSER

OTHER GOVERNMENT

CENTRAL INTELLIGENCE AGENCY
ATTN: KATIE POLEY
ATTN: LAWRENCE TURNBULL, OSWR/NED

U S ARMS CONTROL & DISARMAMENT AGCY
ATTN: A LIBERMAN

DEPARTMENT OF THE INTERIOR
US GEOLOGICAL SURVEY NATIONAL CENTER
ATTN: W LEITH

DEPARTMENT OF DEFENSE CONTRACTORS

APPLIED RESEARCH ASSOCIATES, INC.
ATTN: C J HIGGINS

APPLIED RESEARCH ASSOCIATES, INC.
ATTN: S BLOUIN

APPLIED RESEARCH ASSOCIATES, INC
ATTN: R FRANK

APPLIED THEORY, INC.
2 CY ATTN: J TRULIO

BOEING TECHNICAL & MANAGEMENT SVCS, INC.
ATTN: M/S 87- 60, ROBERT M SCHMIDT

CALIFORNIA INSTITUTE OF TECHNOLOGY
ATTN: T AHRENS

ENSCO, INC.
ATTN: DOUGLAS BAUMGARDT

JAYCOR
ATTN: CYRUS P KNOWLES

KAMAN SCIENCES CORPORATION
ATTN: DASIAC
ATTN: DASIAC/DARE

LOGICON R AND D ASSOCIATES
ATTN: C K B LEE
ATTN: D SIMONS

MAXWELL TECHNOLOGIES INC
ATTN: DR K L MCLAUGHLIN
ATTN: K PYATT
ATTN: R LAFRENZ

PACIFIC-SIERRA RESEARCH CORP.
ATTN: H BRODE

S- CUBED
ATTN: JACK MURPHY

SCIENCE APPLICATIONS INTERNATIONAL CORP
ATTN: R SCHLAUG

SCIENCE APPLICATIONS INTL CORP
ATTN: G EGGUM
ATTN: G PHILLIPS
ATTN: H WILSON
ATTN: L SCOTT
ATTN: T C BACHE, JR
ATTN: W WOOLSON

SCIENCE APPLICATIONS INTL CORP
ATTN: J COCKAYNE

TITAN RESEARCH & TECHNOLOGY DIVISION
ATTN: J THOMSEN

TITAN CORPORATION (THE)
TITAN RESEARCH & TECHNOLOGY DIVSN
ATTN: S SCHUSTER

TRW S. I. G.
ATTN: NORMAN LIPNER

WASHINGTON UNIVERSITY OF
ATTN: J KATZ

WEILDLINGER ASSOCIATES, INC.
ATTN: I SANDLER